ESR Studies of Low Water Content 1,2-Dipalmitoyl-*sn*-glycero-3-phosphocholine in Oriented Multilayers. 1. Evidence for Long-Range Cooperative Chain Distortions

Eva Meirovitch and Jack H. Freed*

Baker Laboratory of Chemistry, Cornell University, Ithaca, New York 14853 *(Received: May 6, 1980)*

ESR studies on a variety of spin probes incorporated into 1,2-dipalmitoyl-*sn*-glycero-2-phosphocholine (DPPC) bilayers are reported. Well-oriented and low water content (2–15 wt %) bilayers were prepared by using a recently developed alignment technique. Both the higher temperature lamellar liquid crystalline $L_\alpha(1)$ phase and the lower temperature biaxial gel phase were studied. In the $L_\alpha(1)$ phase there is considerable fluidity, and while all the probes are ordered to varying degrees they undergo fairly rapid rotational reorientation with $\bar{R}$ (the mean rotational diffusion coefficient) of the order of 0.1×10^9–1×10^9 s^{-1} and with comparable activation energies of the order of 10 kcal/mol. In this phase, headgroup region probes such as PD-Tempone exhibit spectra as a function of angle θ between the magnetic field and the bilayers that are fully consistent with the well-aligned lamellar morphology. However, the hydrophobic probes such as the spin labeled DPPC (7,6-PC) and cholestane (CSL) exhibit a unique powder-type distribution that appears inconsistent with this lamellar morphology or even with random (or Gaussian) distributions due to sample morphology. On the basis of extensive line-shape analyses (including the use of a new slow-tumbling formulation in which θ may be varied) it is shown that satisfactory fits may be achieved only by using a special distribution corresponding to a coherent two-dimensional distribution of local directors. This is consistent with a cooperative distortion wave persisting for time scales long compared to ESR time scales. In particular, since the hydrophobic probes are expected to report on the chain region of the DPPC bilayers, it is argued that these distortion waves involve bends or kinks of the chains, but do not affect the headgroup region in this $L_\alpha(1)$ phase. The implications of these results are also examined from the point of view of measurements by other techniques. It is also shown that similar spectra are obtained from the highly ordered smectic B_c phases of thermotropic liquid crystals implying similar cooperativity. In the biaxial phase the 7,6-PC appears to be immobilized on the ESR time scale, but CSL, which is highly ordered in this phase, is still reorienting at about 10^8 s^{-1}. In both cases evidence of the cooperative distortion mode is found in the less well-resolved spectra. Further evidence from headgroup region probes indicates that this region is now affected by this mode. Significant changes in the hyperfine tensor of probes in this phase is taken as evidence of intermolecular interactions. We have also studied samples using cylindrical tubes as holders. These yield macroscopically unoriented morphologies, with characteristic line shapes commonly observed in previous spin-probe and spin-label studies of biological membranes, but usually interpreted in terms of mixtures of mobile and immobile sites, an interpretation brought into question by the detailed analyses of this work. Details and implications of the slow-tumbling line-shape simulations as a function of θ are also discussed.

I. Introduction

In ESR studies of spin probes dissolved in liquid crystals, the main goal has been to study properties of these ordered phases via their effect on the ESR line shape of the probe. Our studies of thermotropic nematic phases[1] were consistent with the probe molecule reorienting (with fast[1,2] as well as slow[1b,3a] rates) with respect to a uniaxial director. In the case of smectic mesophases one has the additional experimental degree of freedom of being able to tilt the magnetic field relative to the director.[2,4]

These ESR spin-probe studies have revealed characteristics of the dynamic behavior of the probe molecules as well as properties of the surrounding solvent. These include anisotropic diffusion and/or viscosity, deviations from Brownian reorientation, effects due to fluctuating torques, and effects due to slowly relaxing local structure.[1,3] The contribution of the relaxing local solvent structure to the spin relaxation is found to be appreciable in nematic phases[1b] and even more substantial in the uniaxial smectic A and B phases,[4] suggesting increased cooperativity in the motion. Recent theoretical considerations[5] as well as experimental observations[6–8] related to lyotropic smectic phases and to low temperature thermotropic smectics of a more complex nature are suggestive that with increasing complexity of the medium several new features are brought in. Of particular relevance to us are the features on a molecular level and how, through increasing cooperativity, (dynamic) modes may be of a collective nature and may be transmitted to particular solute (probe) molecules. One may, in such studies, take advantage of the variety of spin probes and of the well-developed theories for analyzing ESR line shapes.

We report in this and subsequent papers ESR results on a systematic investigation of 1,2-dipalmitoyl-*sn*-glycero-3-phosphocholine (DPPC)–water mixtures based on the recently published phase diagram of uniformly aligned phospholipid bilayers.[9b,c] For a water content in the range of 0–15 wt %, a low-temperature biaxial gel phase and a high-temperature uniaxial liquid crystalline phase, denoted $L_\alpha(1)$, have been defined on the basis of optical measurements. The experiments described in the present study were mostly done on 2% water content bilayers, and we have used a recently developed technique to obtain large monodomains of DPPC oriented between glass plates.[9] We present in the Experimental Section evidence based mainly on optical methods that our samples are defect free. The interpretation of the macroscopic optical uniaxiality observed by Powers and Pershan et al.[9,10] and by us with defect-free samples is in terms of uniform planar bilayers parallel to the glass surfaces and (for 2% water content structures) is in terms of a homeotropic alignment with the main DPPC chain axes $\hat{d}_c$ parallel to $\hat{n}_m$ (the normal to the glass plates), while the main headgroup axis $\hat{d}_h$ is perpendicular to $\hat{n}_m$ in both the biaxial and $L_\alpha(1)$ phases.[9,10] DPPC is built of two saturated palmitic acid chain residues and a phosphatidylcholine

0022-3654/80/2084-3281$01.00/0

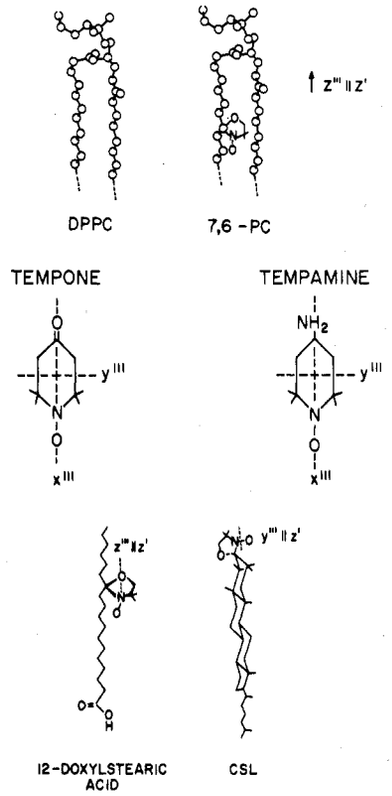

Figure 1. Illustrations of the various spin probe molecules used in this study and of the host DPPC molecule. x''', y''', and z''' are the principal axes of the magnetic tensors, whereas z' denotes the principal axis of the (axially symmetric) ordering tensor.

headgroup; X-ray crystallography[11] and neutron diffraction[12] measurements performed on DPPC bilayers similar to ours showed that $\hat{d}_c \perp \hat{d}_h$ throughout the biaxial and the $L_\alpha(1)$ phases, and, for 2% water content, $\hat{d}_c$ is very nearly parallel to $\hat{n}_m$.

The ESR line shapes indicate that, due to nonzero ordering and motional reorientation, the magnetic tensors of all the nitroxide radicals in the $L_\alpha(1)$ phase are partially averaged. The "hydrophobic" probes we used, 7,6-PC, 12-doxylstearic acid, CSL, and ADL (cf. Figure 1), which are imbedded in the hydrocarbon region of the phospholipid bilayer, are highly ordered, whereas the small and more polar lipid "headgroup" probes, Tempone, PD-Tempone, and Tempamine (cf. Figure 1), are weakly ordered.

We show in Figure 2 various frames of reference appropriate for discussion of our plate sample measurements on the DPPC multilayers. It represents an extension of the frames of reference given by Polnaszek and Freed[1] and Lin and Freed.[4] Thus the x, y, z axes specify the lab frame with $z \parallel \vec{H}$; x''_m, y''_m, z''_m represent the mean director frame for the sample with $z''_m \parallel \hat{n}_m$, where $\hat{n}_m$ denotes the normal to the glass plates, and x''_m lies within the plane defined by $\hat{n}_m$ and $\vec{H}$. We also introduce the local director $\hat{n}_l(\vec{r})$ and its coordinate frame: $x''_l(\vec{r}), y''_l(\vec{r}), z''_l(\vec{r})$ which is a function of the location, $\vec{r}$, in the sample in order to represent fluctuations about the mean. In the absence of any spatial variation in the director, the x''_l, y''_l, z''_l axes are identical with x''_m, y''_m, z''_m. We also require axes specifying the orientation of the probe molecule. They are the principal axes of ordering (and of diffusion): x', y', z' as well as the principal axes of the **A** and **g** tensors: x''', y''', z'''.

The ESR spectra of PD-Tempone and Tempamine are relatively sharp triplets with a monotonically increasing splitting and line widths that depend upon the angle of

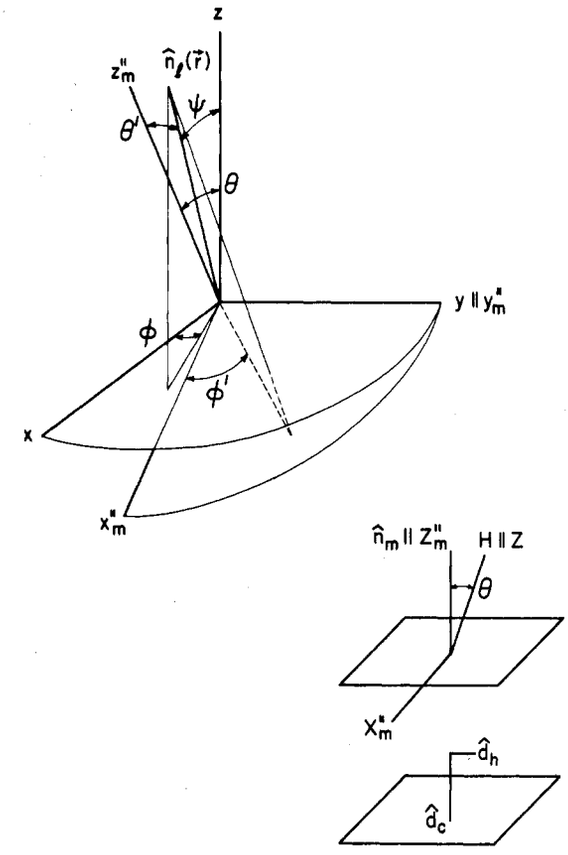

Figure 2. Illustration of the various coordinate frames related to the plate samples. x_m'', y_m'', z_m'' denotes the mean director frame with $z_m'' \| \hat{n}_m$, the plate normal, and x_m'' within the plane defined by z_m'' and **H**; x, y, z denotes the lab frame with $z \| \vec{H}$, θ is the experimentally variable angle between **H** and $\hat{n}_m$. $\hat{d}_c$ denotes the orientation of the undistorted chains and $\hat{d}_h$ the main symmetry axis of the headgroup.

tilt of the field from $\vec{H} \parallel \hat{n}_m$ to $\vec{H} \perp \hat{n}_m$. This is a common "smectic A-type" behavior[4] implying uniform uniaxiality, i.e., $x''_l(\vec{r}), y''_l(\vec{r}), z''_l(\vec{r})$ coincides with the x''_m, y''_m, z''_m frame throughout the sample. By means of a full lineshape analysis one may derive the correlation time(s) for overall reorientation, the extent (and symmetry) of the ordering, the extent of anisotropy in the diffusion, and viscosity tensors.

However, the ESR spectra of the hydrophobic probes display a very particular powder-type feature, indicative of an additional mode, frozen on the ESR time scale, which is characterized by a distribution in z''_l axes with respect to z''_m. We have determined by means of detailed lineshape analysis the form of the distribution function describing this disorder. We interpret this mode in terms of a defect or bend of the chain that exists at some position along the otherwise all-trans aliphatic DPPC chain and such that this defect exists through the medium in the form of a collective wave that is static or else propagates slowly. Furthermore, there must be strong lateral cooperative forces between the adjacent DPPC chains and the probe molecules.

The ability to discriminate such a distribution function was due to the uniform alignment of the phospholipid bilayers. Clearly it was necessary to subject the ESR line shapes to detailed analysis to come to such a conclusion. This detailed analysis also yields information on the microscopic dynamic properties of the probes as we discuss below.

In section II we present experimental details regarding sample preparation. In section III we discuss our results, describing the spectral simulations in some detail. Re-

marks on the relation to other work appear in section IV, while conclusions are given in section V.

II. Experimental Section

(A) *Sample Preparation.* DPPC was purchased from Sigma and its purity checked routinely by means of standard methods (such as, for example, the gel-liquid crystalline phase transition temperature of a phospholipid dispersion in excess of water). Deionized water was added to the solid, dry phospholipid to obtain equilibrated mixtures with the appropriate water content (usually 2 wt %).[9] The various spin labels were added by precise weighing to a final concentration of 10^{-3} M. From this mixture we prepared multilayers oriented between glass plates following the procedure of Powers and Pershan.[9] This method consists of treating clean glass surfaces with a surfactant agent (we used hexadecyltrimethylammonium bromide obtained from Aldrich), which is known to induce homeotropic alignment of the phospholipid molecules. Then the "sandwich" samples were introduced into cylindrical sample holders; the air was exchanged for nitrogen; and subsequently the assembly was heated slowly to the upper end of the $L_\alpha(1)$ phase ($\approx$125 °C) to anneal defects and to deoxygenate the DPPC bilayers. The temperature was then lowered slowly to 85–90 °C for about 12 h to complete deoxygenation (see comments below) and finally lowered to the range investigated experimentally. When this method was used for 2 wt % water content bilayers, 1.5 cm × 0.7 cm highly oriented monodomains of a thickness of 150 ± 50 μm were obtained. The surface of the bilayer in a particular sample was less than 70% of the glass surfaces to avoid edge misalignment.

Several higher water content samples were also prepared in this work. These can be obtained, according to the method of Powers and Pershan,[9a,c] by immersing the 2 wt % water content sample into deionized water for given periods of time. However, this procedure has to be modified to obtain well-aligned and completely deoxygenated bilayers with a constant water content and doped with a known concentration of spin probe molecules, such as required for high-resolution ESR experiments. We do not have at this stage a refined method to achieve this. We are currently developing a method for achieving this using an alignment technique developed recently by Asher and Pershan[10a] which does not require the high annealing temperatures of the Powers and Pershan[9] technique.

Nevertheless, several samples with a water content higher than 2 wt % were prepared by the same method used for monohydrate bilayers; only a few samples, aligned sufficiently well, were used for short ESR experiments at relatively low temperature to prevent dehydration.

Dehydration of the monohydrate occurs only under drastic conditions[13a] and no problems regarding the constancy of the water content were encountered.

Deoxygenation could become important, especially when using PDT in the $L_\alpha(1)$ phase. From our previous experience with thermotropic liquid crystals, heating in a nitrogen atmosphere for several hours is an efficient deoxygenation procedure. We cannot say at this stage whether the deoxygenation was indeed complete in the phospholipid bilayers. However, the PDT lines at the higher temperatures, where the lines are relatively narrow, were further narrowed by this treatment.

The criterion for establishing whether a particular sample is defect-free has been adopted from a recent work of Asher and Pershan[10a] who employed polarizing microscopy to study defects induced into DPPC bilayers. Complete extinction of light when the sample is placed between two crossed polarizers was considered to be a reliable indication of good alignment and absence of defects (see Figure 3a of ref 10b). Based also on our previous discussion in section I, we conclude that our 2 wt % water content samples were well oriented, mainly defect-free with the lipid chains on the average perpendicular to the glass plates.

With the technique described above we obtained, in most cases, samples with virtually identical ESR spectra at the same temperature and with relatively narrow lines. Significant changes in the line width (up to a factor of 2.5) from 4 to 115 °C were observed with these samples. These variations were reproducible upon increasing or decreasing the temperature between room temperature and 115 °C and were virtually the same for all the good samples. Careful line-shape analysis indicates that the extent of static inhomogeneous broadening due to misalignment of the mean director parallel to $\hat{n}_m$ is small relative to other effects which determine the ESR line shape.

(B) *Spectrometer.* An E-12 Varian X-band (3.3 kG) spectrometer equipped with a Varian 257 temperature control accessory was used. The temperature was controlled by using a copper–constantan thermocouple placed just above the sample. The accuracy of the absolute temperature was estimated at ±1 °C although the temperature could be controlled more accurately (±0.25 °C).

The spectrometer settings were chosen so that the microwave power was far below saturation, the modulation amplitude was less than one-tenth of the line width, and the modulation frequency was 10 kHz for PDT and Tempone and 100 kHz for all the other spin probes.

(C) *Spin Probes.* 7,6-PC was obtained from Professor G. W. Feigenson of the Department of Biochemistry and Molecular and Cell Biology at Cornell University. This probe was synthesized from lysolecithin and acylated with a specifically labeled fatty acid according to the procedure of McConnell[14a] with the label group on C-8 on the sn_2 chain.

12-Doxylstearic acid, CSL, and ADL were purchased from Synvar.

Tempamine [4-amino-2,2,6,6-tetramethylpiperidinyl-1-oxy] was purchased from Molecular Probes.

PD-Tempone was prepared by the method of Rozantsev[14b] for Tempone as described previously.[3b]

III. Results and Discussion

The ESR spectra of the small and relatively polar probes Tempone, PD-Tempone, and Tempamine are characteristic of weakly ordered solute molecules in a uniaxial medium, i.e., a sharp triplet with a monotonic variation in the mean hyperfine splitting and in the g shift upon tilting the field relative to the director. On the other hand, the ESR spectra of the large "hydrophobic" probes 7,6-PC, 12-doxylstearic acid, CSL, and ADL reflect a very particular angular-dependent distribution of $\hat{n}_l(\vec{r})$ relative to $\vec{H}$. We shall discuss these two classes of probes separately below.

(A) *Small and Polar Probes.* We note first of all our unique observation that Tempone, PD-Tempone, and Tempamine yield ESR spectra arising *solely* from the probe in the lipid region of the phospholipid bilayer. In more usual cases they are distributed between an aqueous phase and lipid phase with greater solubility in the former due to their high solubility in water.[15] The 2 wt % water content mixtures are in fact DPPC monohydrates where the water molecules are most likely bound to the phospholipid headgroups.[13a,15a,16] The low water content DPPC bilayers are thus particularly appropriate for studying the hydrocarbon region of the bilayer, using these types of probes.

TABLE I: Magnetic Tensors

	a_N	a_x'''	a_y'''	a_z'''	$a_N{}^c$ isotropic
CSL in $L_\alpha(1)$	14.1	6.2	6.2	30.00	14.5
CSL in the biaxial phase	15.5	6.2	6.2	33.00	
7,6-PC[a] in $L_\alpha(1)$	14.24	5.89	5.42	31.42	14.3
7,6-PC in the biaxial phase	16.3	8.0	8.0	33.0	
12-doxylstearic acid[a] in $L_\alpha(1)$	14.24	5.89	5.42	31.42	14.3
PD-Tempone[b] in $L_\alpha(1)$	15.07 $g_N = 2.0099$	5.72 $g_x''' = 2.0062$	5.11 $g_y''' = 2.00215$	34.37 $g_z''' = 2.00500$	15.07

[a] The principal values of the a and g tensors were adopted from ref 17. [b] The principal values of the hyperfine tensor were obtained by a scaling procedure from ref 4a as explained in the text: the g tensor values were taken from ref 4a without further change. [c] The hyperfine splitting for the various probes measured in the isotropic phase occurring above $L_\alpha(1)$.

TABLE II: Ordering Parameters and Diffusion Rates

	T, °C	$\langle D^2_{00}\rangle$	λ^a	$10^{-8}R_\perp$,[b] s^{-1}	N^b	E_{act}, kcal/mol
12-doxylstearic acid in $L_\alpha(1)$	117	0.16	1.1	6.77	4.0	
	107	0.21	1.4	5.0	4.0	9.0 ± 1.0
	90	0.25	1.7	2.8	4.0	
7,6-PC in $L_\alpha(1)$	115	0.28	1.9	3.5	2.0	
	105	0.31	2.1	2.5	2.0	10.0 ± 1.0
	95	0.34	2.4	1.7	2.0	
CSL in $L_\alpha(1)$	116	0.645	5.0	8.9	5.0	
	107	0.67	5.3	6.8	5.0	9.0 ± 1.0
	92	0.68	5.5	4.2	5.0	
CSL in the biaxial phase	70	0.83	9.5	5.5	5.0	
	40	0.86	10.6	2.0	5.0	7.0 ± 1.0
	25	0.87	11.0	1.1	5.0	

	T, °C	$\langle D^2_{00}\rangle$	λ	ρ	$10^{-8}R_\perp$, s^{-1}	N	$\hat{N}$	E_{act}, kcal/mol
PD-Tempone in $L_\alpha(1)$	115	0.11	0.82	−0.25	5.5	1.00	6.0	9.5 ± 1.0
	90	0.11	0.82	−0.25	2.35	1.00	6.0	

[a] $\langle D^2_{00}\rangle \equiv e^{\lambda\cos^2\Psi}$; the accuracy in λ is ±10%. [b] The accuracy in $R_\perp$ and N is ±20%.

The smectic A-type behavior of Tempone, PD-Tempone, and Tempamine illustrated in Figure 3a for PD-Tempone is straightforward evidence for the microscopic uniaxiality of the immediate environment of these solutes. As we discuss in detail below, the hydrophobic probes report on a local environment with a symmetry lower than uniaxial. These different observations most likely reflect the heterogeneity of the bilayer, due to the fact that "polar" and "hydrophobic" probes are located at different depths in the bilayer. We obtain a consistent picture if we assume that the small polar probes are located within the region of the bilayer near the headgroup interface; the relatively large values, obtained with PD-Tempone for a_N the isotropic hyperfine splitting (cf. Table I and below), support this assumption of a relatively polar environment.[4a,17] This region of the bilayer is then uniaxial such that $\hat{n}_l(\vec{r})$ is parallel to the mean director $\hat{n}_m$. [One might inquire whether these weakly ordered "headgroup" probes would be sensitive to the bilayer heterogeneity. Actually, one predicts that the PD-Tempone spectra (for 2–9 wt % water) would be very sensitive to the types of distribution sensed by the hydrophobic probes (cf. section IIB) if they were present. This is illustrated by the theoretical prediction in Figure 3a.]

PD-Tempone was found to exhibit asymmetric ordering in the $L_\alpha(1)$ phase. To obtain the ordering parameters $\langle D^2_{0,0}\rangle$ and $\langle D^2_{2,0} + D^2_{-2,0}\rangle$ one has to measure experimentally both the mean hyperfine splitting $\langle a\rangle$ and the $\langle g\rangle$ value corresponding to the $\theta = 0°$ spectra. We have performed g and a measurements for several temperatures and obtained approximately temperature independent values of $\langle g\rangle = 2.00593$ and $\langle a\rangle = 14.6$ G for $\theta = 0°$. Using eq 3a and 3b of ref 4a we calculated the ordering parameters $\langle D^2_{0,0}\rangle_i$ and $\langle D^2_{2,0} + D^2_{-2,0}\rangle_i$ with i denoting x''', y''', or z''', given in Table II.

The principal values of the magnetic tensors for PD-Tempone in the $L_\alpha(1)$ phase of DPPC, given in Table I, were obtained by scaling the corresponding values of PD-Tempone in phase V[4a] by $a_N(\text{DPPC})/a_N(\text{phase V})$ where $a_N(\text{DPPC}) = 15.07$ G is the value measured in the isotropic phase occurring above the $L_\alpha(1)$, while $a_N(\text{phase V}) = 14.78$ G. [Note that a_N in hydrocarbon solvents is about 14.3 G.[4a]] We could not measure $A_{z'''}$ from rigid-limit spectra since PD-Tempone "plated out" upon decreasing the temperature below about 10 °C. The ordering parameters obtained in this manner were then used for a complete line-shape simulation for $\theta = 0°$ and good fit with the experiment, illustrated in Figure 3b, was only obtained for $i = y'''$. The fact that the entire line shape, which is sensitive to the ordering in this region, was well reproduced with the magnetic parameters obtained as described above indicates that the scaling procedure is adequate for PD-Tempone in the $L_\alpha(1)$ phase.

We found with complete line-shape analysis of the $\theta = 0°$ spectra of PD-Tempone for various temperatures in the $L_\alpha(1)$ phase, using the analysis method of Freed and coworkers,[1-4] that this probe is weakly ordered about y''' with an asymmetric ordering potential $\lambda = 0.82$, $\rho = -0.25$ from 90 to 118 °C. We were able to fit the results with a model of isotropic diffusion and anisotropic viscosity with $\hat{N} = \hat{R}_\parallel/\hat{R}_\perp = 6.0$ ($\hat{R}_\parallel$ and $\hat{R}_\perp$ denote the principal values of the axially symmetric viscosity tensor) over this temperature range. This apparent anisotropic viscosity may perhaps be more correctly fit by a model of slowly relaxing local structure.[1,4] These results are consistent with the observations of PD-Tempone in smectic A phases of thermo-

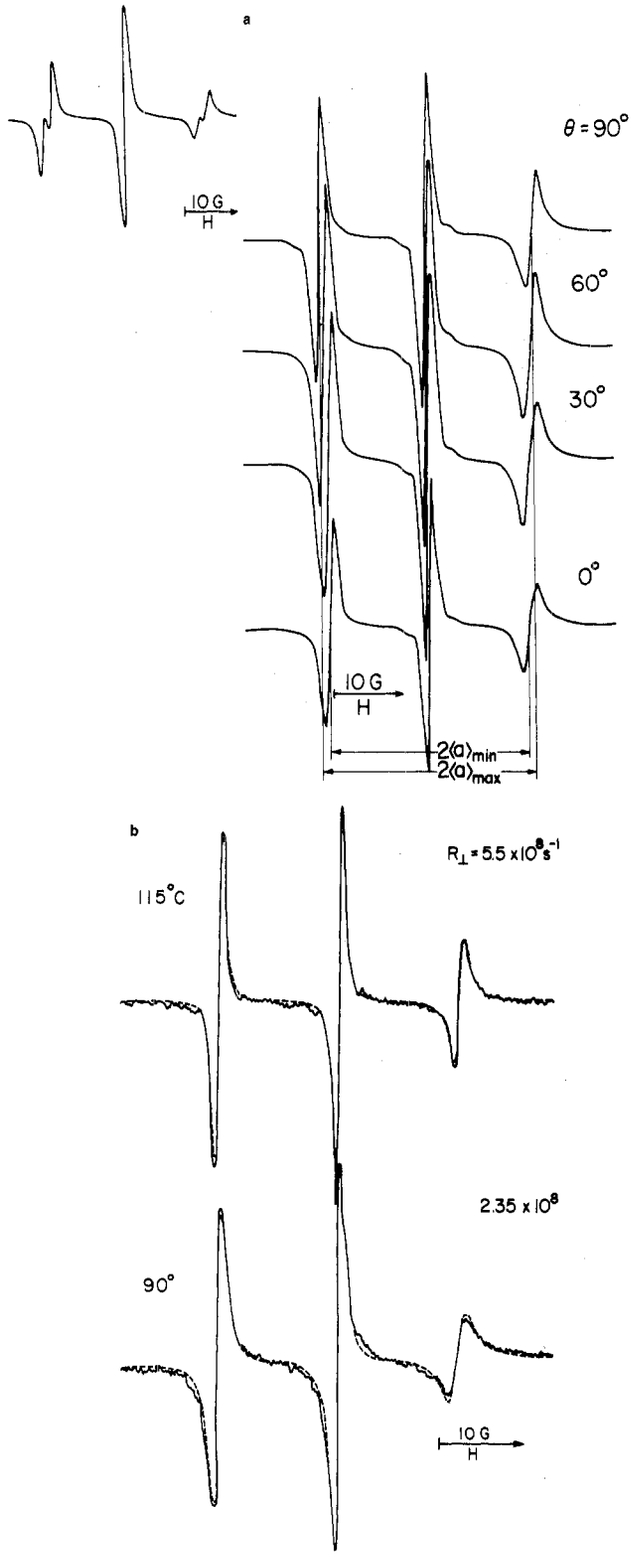

Figure 3. (a) ESR spectra of 10^{-3} M PD-Tempone dissolved in 9% water content DPPC bilayers in a 150-μm thick sample in the $L_\alpha(1)$ phase at 75 °C at various orientations of the field as denoted in the figure; insert shows spectrum *calculated* by using distribution of eq 1 with other spectral parameters estimated from experimental figure for $\theta = 0°$. (b) Experimental ESR spectra of 10^{-3} M PD-Tempone in 2 wt% water content DPPC bilayers in a 150 ± 50 μm thick plate sample at various temperatures in the $L_\alpha(1)$ phase for $\theta = 0°$ (——), calculated spectra with $\lambda = 0.82$, $\rho = -0.25$, $T_2^{*-1} = 0.3$ G, $N = 1.0$, $\hat{N} = 6.0$, and $R_\perp$ as denoted in the figure.

tropics.[4a]

We have found that the line positions (i.e., splittings) of the spectra in Figure 3b for all values of θ are consistent with this detailed analysis, but we have not analyzed the

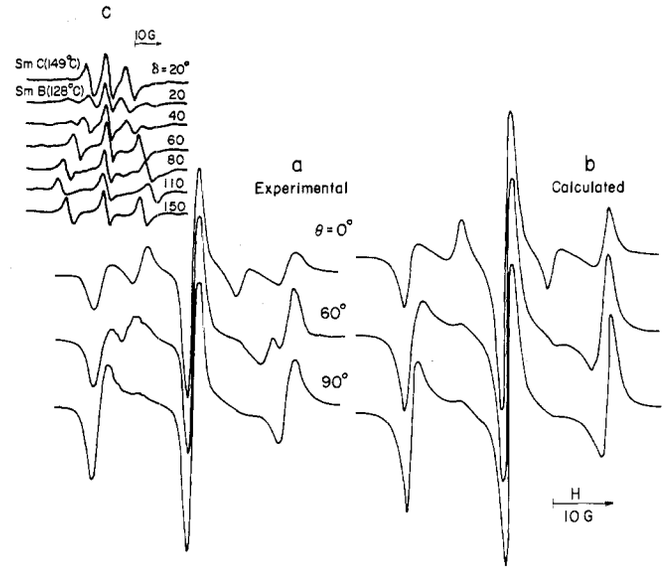

Figure 4. (a) Experimental ESR spectra of 10^{-3} M CSL dissolved in 2 wt% water content DPPC bilayers in a 150 ± 50 μm thick plate sample in the $L_\alpha(1)$ phase (107°) with θ, the angle between H and the plate normal $\hat{n}_m$, as denoted in the figure. (b) Calculated spectra with $\lambda = 5.3$, $\rho = 0.0$, $R_\perp = 6.8 \times 10^8$ s^{-1}, $N = 5.0$, and the principal values of the magnetic tensors from Table I. The T_2^{-1} values for 107 °C are given in Table III, based partly on the theory of Moro and Freed.[4b] The spectra corresponding to the various orientations Ψ were superimposed by using eq 1. (c) ESR signals of the cholestane spin probe in the smectic B_C phase (at 128 °C) of TBBA in a glass plate sample as function of the orientation of the magnetic field H. δ is the angle between H and the normal to the glass plates. The thickness of the mesogen was about 30 μm. The smectic C was obtained by first allowing the mesogen to cool from the nematic phase to the smectic A phase in a strong (21 kg) magnetic field perpendicular to the glass plates and then cooling further to the smectic phase (upper spectrum) with the magnetic field tilted by about 20° to the normal to the plate.

$\theta \neq 0°$ spectra further for several reasons. They are (1) the great sensitivity of the $\theta \neq 0°$ line shapes to inhomogeneities due to sample mosaicity as well as magnetic-field effects,[4a,c] as well as (2) the present formulation of Moro and Freed[4b] for analyzing such spectra for all tumbling rates has yet to be extended to nonaxial molecular ordering.

For Tempamine we found basically the same "smectic A-type" behavior in the $L_\alpha(1)$ phase and preliminary line-shape analysis indicates weak x''' ordering with $R_\perp$ of the order of 10^8–10^9 s^{-1}.

(*B*) *Large Hydrophobic Probes.* The ESR spectra of 7,6-PC, 12-doxylstearic acid, CSL, and ADL are orientation dependent, i.e., they depend upon the angle θ between $\vec{H}$ and $\hat{n}_m$ (cf. Figures 4–8). The angular dependence of the line shapes is consistent with the fact that the sample is macroscopically oriented and the probes are microscopically partially ordered with respect to $\hat{n}_l(\vec{r})$. In particular, for 7,6-PC and 12-doxylstearic acid, we have $z''' \equiv z'$, since z''' is parallel to the long molecular axis z' which tends to align along z_l''. For similar reasons $y''' \equiv z_l''$ for CSL and ADL (see Figures 1 and 2). An important feature reflected in the spectra, discussed below, is that there is a distribution of z_l'' axes relative to the x_m'', y_m'', z_m'' frame giving rise to a distribution in the angle Ψ between z_l'' and $\vec{H}$ with $\cos \Psi = \cos \theta \cos \theta' - \sin \theta \sin \theta' \cos \varphi'$ (cf. Figure 2).

In order to simulate the experimental line shapes in Figures 4–8 one has to consider effects of (1) homogeneous line broadening due to overall molecular reorientation and (2) further line broadening of an inhomogeneous nature due to static distributions. We have first attempted to simulate the line shapes for $\theta = 0°$ by assuming that the main effect is of a dynamic nature, with the following

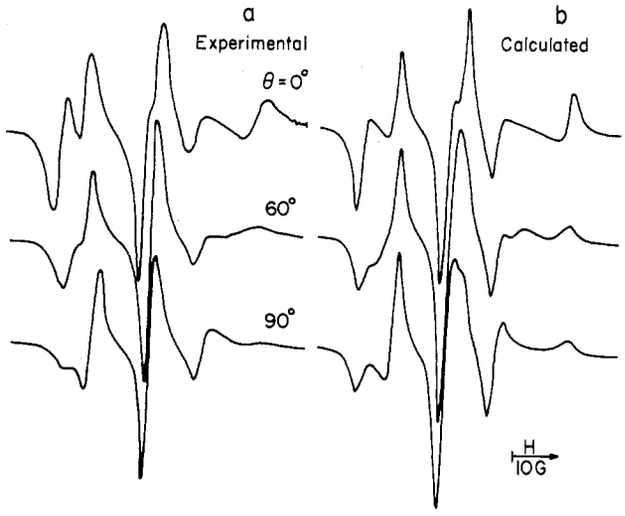

Figure 5. (a) Same as Figure 4a for 7,6-PC corresponding to 115 °C. (b) Same as Figure 4b with $\lambda = 2.07$, $\rho = 0.0$, $R_\perp = 2.5 \times 10^8$ s^{-1}, $N = 4.0$, and T_2^{-1} given in Table III.

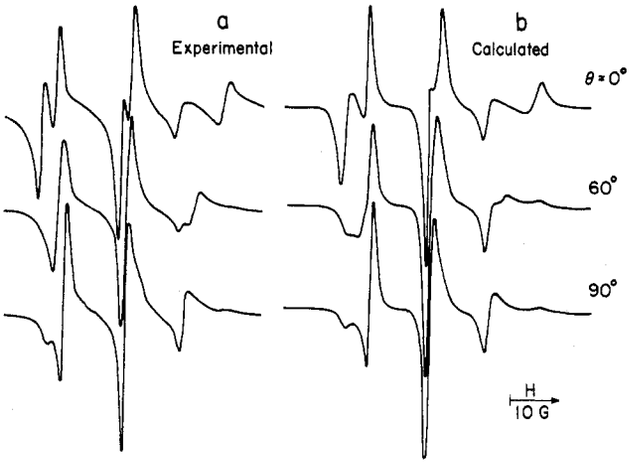

Figure 6. (a) Same as Figure 4a for 12-doxylstearic acid to 107 °C. (b) Same as Figure 4b with $\lambda = 1.4$, $\rho = 0.0$, $R_\perp = 5 \times 10^8$ s^{-1}, $N = 2.0$, and T_2^{-1} given in Table III.

model:[18] $z_l'' \parallel z_m''$ everywhere but the principal axes of orientation, x', y', z' are tilted relative to the magnetic frame x''', y''', z''' with θ''', φ''' denoting the polar and aximuthal angles of z' in the x''', y''', z''' frame. Starting with a nitroxide radical undergoing fast reorientation (with a rate $R_\parallel$ s^{-1}) about z' and very slow reorientation (with a rate $R_\perp$ s^{-1}) about axes perpendicular to z', we allowed for a gradual increase in $R_\perp$ over the entire dynamic range for arbitrary values of θ'''. We could not reproduce the $\theta = 0°$ spectra with this model and could not conceive of any simple "single mode" dynamic model likely to explain the spectra (note that the effect of varying φ''' is small for $z' \parallel z'''$ due to the near axial symmetry of the magnetic tensor in the ordering frame).

The other extreme approach, which would be to assume that the line shapes are mainly determined by a particular type of a constant static distribution of immobilized nitroxides, can be definitely ruled out. Even without referring to the liquid crystalline nature of the $L_\alpha(1)$ phase, which is inconsistent with having immobilized solute molecules, it can be shown by general arguments based on the values of the extreme splittings observed experimentally which are reduced relative to the values of the magnetic parameters of a static nitroxide that such a model is not plausible for any radical in the $L_\alpha(1)$ phase, as well as for CSL in the biaxial phase. Thus at least some motional averaging has to take place.

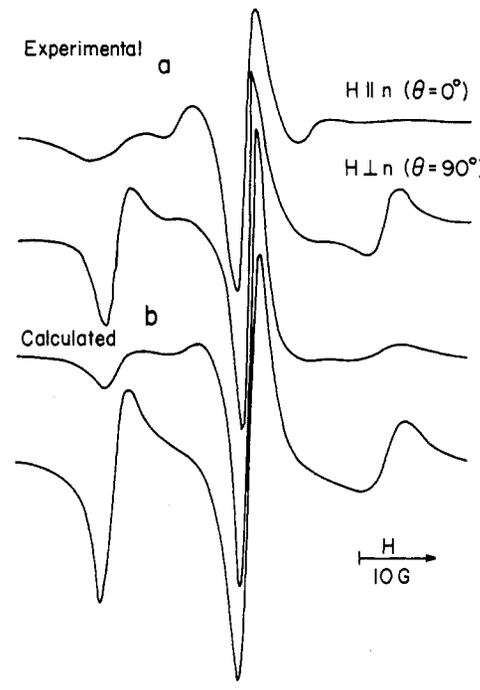

Figure 7. (a) Same as Figure 4a for CSL in the biaxial phase at 40 °C. (b) Same as Figure 4b with $\lambda = 10.6$, $\rho = 0.0$, $R_\perp = 2.0 \times 10^6$ s^{-1}, $N = 5.0$, and T_2^{-1} given in Table III.

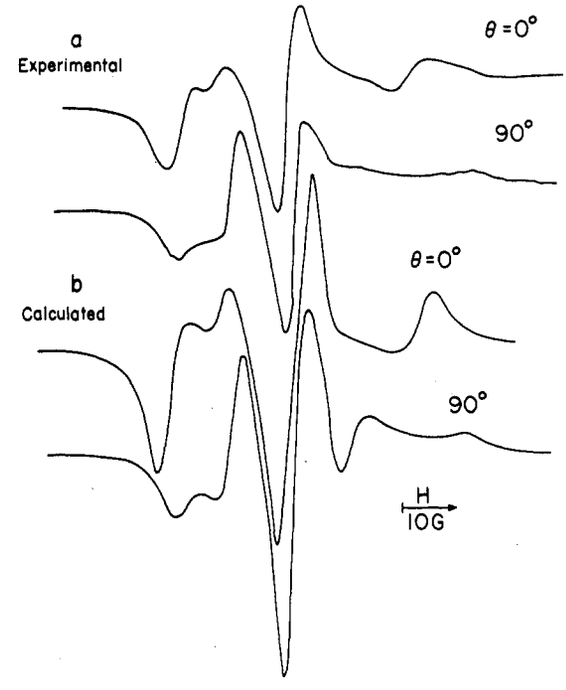

Figure 8. (a) Same as Figure 4a for 7,6-PC in the biaxial phase at 40 °C. (b) Same as Figure 4b with $\lambda = 3.8$, $\rho = 0.0$, $R_\perp = 2.0 \times 10^5$ s^{-1}, $N = 4.0$, and T_2^{-1} given in Table III.

We therefore conclude that the basic features of the spectra can be explained only by considering the combined effects of both dynamic (homogeneous) and static (inhomogeneous) line-broadening phenomena consistent with a uniform lamellar phase. The line-shape analysis shows that the dynamic contribution comes from overall molecular reorientation, and the static contribution is due to a two-dimensional (2D) spatial distribution of $\hat{n}_l(\vec{r})$, which we interpret as arising from collective distortions of kinks in the DPPC chains transmitted through lateral interactions to the aliphatic chains of DPPC, 7,6-PC, and 12-doxylstearic acid and also to the rigid probes CSL and ADL. The rationale of the analysis is as follows. For θ

= 0° the x_m'', y_m'', z_m'' and the x, y, z and therefore the distribution of $\hat{n}_l(\vec{r})$ relative to $\vec{H}$, which can be derived directly from the ESR spectrum, gives also the distribution of $\hat{n}_l(\vec{r})$ relative to $\hat{n}_m$. The ESR line shapes for any orientation θ are then calculated by using this distribution function with the line shapes for the individual components (corresponding to particular values of Ψ) obtained by using the new computer formulation of Moro and Freed[4b] for calculating ESR line shapes as a function of the relative orientation of a uniaxial director and the magnetic field.

We shall divide the subsequent discussion into two parts. First we consider the static broadening effects and then we concentrate on the dynamic effects.

(1) Line Broadening due to Static Distributions. We consider first the $\theta = 0°$ spectrum of CSL. The line widths for the individual components for each Ψ in the powder-type spectra will be discussed below, and we shall focus on the shape of the distribution function used to superimpose these spectra in order to obtain the final ESR line shape. We notice that the $\theta = 0°$ spectra are different from the common isotropic three-dimensional (3D) powder spectra in that the relative intensities of the $\theta' = 0°$ and $\theta' = 90°$ spectral regions are almost equal, and this is in disagreement with the spectra for an isotropic powder (see ref 19 and 20, p 200) which yields a greater intensity for $\theta' = 90°$ than for $\theta' = 0°$. The distribution function $P(\theta',\varphi')$ for an isotropic three-dimensional distribution of orientations is $P(\theta',\varphi') \sin\theta' \, d\theta' \, d\varphi' = (1/4\pi) \sin\theta' \, d\theta' \, d\varphi'$.

We note that for a well-aligned smectic A-type of spectrum one would have[4a] $P(\theta',\varphi') \sin\theta' \, d\theta' \, d\varphi' \propto e^{-\alpha \sin^2\theta'} \sin\theta' \, d\theta' \, d\varphi'$ where $\alpha \to \infty$ as the alignment becomes perfect. One may therefore attempt such a Boltzmann distribution with a finite α to represent a *random* static distribution. In particular, for $\alpha \approx 1.5$ it is possible to equalize the intensities for the $\theta' = 0$ and 90° regions as shown in Figure 9a for CSL. This would represent an unusually low ordering, e.g., a very large mosaicity inconsistent with the PD-Tempone results, optical observations, etc. However, we could *not* reproduce the very unique steep features between the two peaks of a particular hyperfine component as shown in Figure 9c. We even examined distribution functions of form $P(\theta',\varphi') \propto e^{-(\alpha \sin^2\theta' + \beta \sin^4\theta')}$ allowing for two adjustable parameters but we could not improve the fit appreciably. [The optimum values were $\alpha \approx 1.7$, $\beta \approx -0.7$.]

The only form for $P(\theta',\varphi')$ which is found to clearly reproduce these features is

$$P(\theta',\varphi') \propto 1/\sin\theta' \tag{1}$$

which has the character of an isotropic two-dimensional (2D) distribution.[21] Let us see how this comes about. Suppose $\hat{n}_l(\vec{r})$ is of the form of a coherent wave such that

$$n_{l,z_m''} = \cos\theta' = \cos\frac{2\pi}{P}y_m'' \tag{2a}$$

$$n_{l,x_m''} = \sin\theta' = \sin\frac{2\pi}{P}y_m'' \tag{2b}$$

i.e., $\hat{n}_l(\vec{r})$ is oscillating in the x_m'', z_m'' plane with wavelength or pitch P along the y_m'' axis. Then the range of y_m'' values (between y_m'' and $y_m'' + \delta y_m''$) which correspond to a particular value of $n_{l,z_m''}$ is

$$P(\theta') \propto \delta y_m'' = \delta(\cos\theta') \left[\frac{dn_{l,z}}{dy_m''}\right]^{-1} = -\frac{P}{2\pi}\delta(\cos\theta') \frac{1}{\sin\frac{2\pi}{P}y_m''} \propto \frac{1}{\sin\theta'} \tag{3}$$

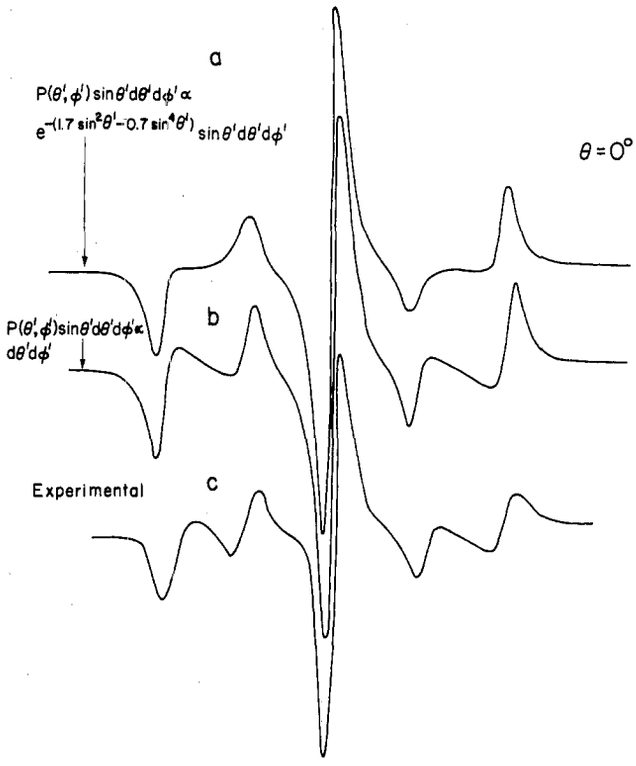

Figure 9. (a) Calculated ESR spectra as explained in the captions of Figure 4b with $P(\theta',\varphi') \propto e^{-(1.7\sin^2\theta' - 0.7\sin^4\theta')}$. (b) Same as a but $P(\theta',\varphi') \propto (\sin\theta')^{-1}$. (c) Experimental spectrum for $\theta = 0°$ shown in Figure 4a.

Now eq 1 implies a random distribution in φ', so that we must modify eq 2 to

$$n_{l,z_m''} = \cos\theta' = \cos\left(\frac{2\pi}{P}y_l''\right) \tag{4a}$$

$$n_{l,x_m''} = \sin\theta' \cos\varphi' = \sin\left(\frac{2\pi}{P}y_l''\right)\cos\varphi' \tag{4b}$$

$$n_{l,y_m''} = \sin\theta' \sin\varphi' = \sin\left(\frac{2\pi}{P}y_l''\right)\sin\varphi' \tag{4c}$$

where φ' is randomly distributed in different parts of the sample, and $y_l''(\vec{r})$ lies in the plane of x_m'', y_m''. Equation 3 now applies for each region of the sample, so that eq 1 results.

The spectral simulations for all the hydrophobic probes (including homogeneous line-broadening effects to be discussed below) for $\theta = 0$, 30, 60, and 90°, using eq 1, are illustrated in Figures 4–8. The $\theta \neq 0°$ orientations are less sensitive to the shape of $P(\theta',\varphi')$ than the $\theta = 0°$ spectrum; however, for any value of θ, the use of eq 1 gave a better fit than any of the Boltzmann distribution forms.

Thus we conclude that our results are clear evidence for a cooperative wavelike phenomenon as distinct from some *random* distribution. [In particular the choice of the Boltzmann distribution with $\alpha = 1.7$, $\beta = -0.7$ very nearly reproduces the distribution of eq 1 for $\theta' > 10°$. Its failure to predict the detailed line shape must therefore be due to the contributions from $\theta \approx 0$–10° for which $\lim_{\theta' \to 0} (\sin\theta')^{-1} = \infty$ while any Boltzmann distribution with a reasonably finite number of terms remains finite.] We also note that, while the $\theta = 0°$ spectra would not distinguish between eq 2 and 4, those for $\theta \neq 0°$ and, in particular, $\theta = 90°$ would. The form of eq 4 is thus supported by the good fits of the $\theta = 90°$ spectra. Furthermore, we have

found that for the distribution of eq 1 we must let θ' range between 0 and 90°, i.e., any cutoff of the distribution for $\theta'_{max} < \sim 84°$ is inconsistent with the observed spectra.

Line shapes similar to our $\theta = 0°$ spectra have been observed by Luckhurst et al.[21] in an ESR study of a cholesteric phase doped with CSL and interpreted in terms of macroscopically aligned helix axes of the cholesteric structure that are perpendicular to $\vec{H}$ in agreement with theory. Meirovitch et al.[22] observed similar spectra in a twisted smectic C monodomain doped with CSL which is morphologically identical with the cholesteric example. It is thus tempting to assign the particular type of distribution reflected in our spectra to an appropriate macroscopic configuration of the DPPC bilayers. However, as noted above and discussed in detail below (section IV), any morphology except for the bilayer structure is unacceptable. Thus, we shall search for a microscopic morphological effect. [One can also show that simple models such as a two-site model, which would correspond, for example, to an alternating smectic C structure are inconsistent both with our results and with other physical measurements.]

Fast kink diffusion along the aliphatic chain residues of thermotropic smectic liquid crystals has been invoked by Hsi et al.[23] in interpreting their ^{2}H NMR results on selectively deuterated (in the chain region) mesomorphic molecules. According to the model suggested by these authors, at a particular position along the initially all-trans aliphatic chain, there is a finite probability for the formation of an even or a gauche kink, which is the simplest and most common defect referred to in the literature.[24] It leads to two additional orientations of the methylene C–D bond corresponding to $\Psi \simeq 50$ and 20°, besides the orientation $\Psi \simeq 90°$ for the undeformed chain (recall that for $\theta = 0°$ one has $\Psi = \theta'$). Fast (on the ^{2}H NMR time scale) kink diffusion then implies fast equilibration between these three sites (the relative populations of which depend upon the position of the particular "deformed" C–D bond along the chain, since the probability of a deformation increases monotonically in the direction of the end-methyl group). The NMR spectrum is then a time-averaged spectrum. "Slow" kink diffusion would then result in the static limit, and the NMR spectrum would be given by the superposition of three properly weighted spectra, corresponding to the three distinct sites.

There is extensive experimental evidence that in the higher water content $L_\alpha(2)$ phase kink diffusion is fast, even on the ESR time scale.[17,25] Let us assume that the model of Hsi et al.[23] applies for the fatty acid residues of the phospholipid molecules in the $L_\alpha(2)$ phase and upon crossing the $L_\alpha(2) \rightarrow L_\alpha(1)$ phase transition this process is appreciably slowed down. In our ESR spin probe experiments using for example, 7,6-PC, the hyperfine tensor of the nitroxide radical is the reporting group. A quick examination of the molecular conformation of 7,6-PC shows that the local director $\hat{n}_l(\vec{r})$ will correspond for $\theta = 0°$ to $\Psi = 0°$ in an undistorted chain and to $\Psi = 40$ and 70° in distorted chains. We found that we *cannot* interpret our powder-type ESR line shapes assuming that the disorder arises from a superposition of these three distinct sites. Rather, the ESR spectra reflect a *uniform* distribution of sites in the range $0° \leq \Psi \leq 90°$. For such a uniform distribution the kink diffusion process would have to become an averaging mechanism over a continuum of equally probable sites. We shall denote this as a "continuous chain distortion or kink mode". It then becomes essentially the same as the concept of reptation[26] (which can be envisaged either as a deformation proceeding continuously in the course of time along a single aliphatic chain or as a defect wave propagating through the medium) introduced by de Gennes[26a] and well-accepted today when dealing with polymer chain dynamics.

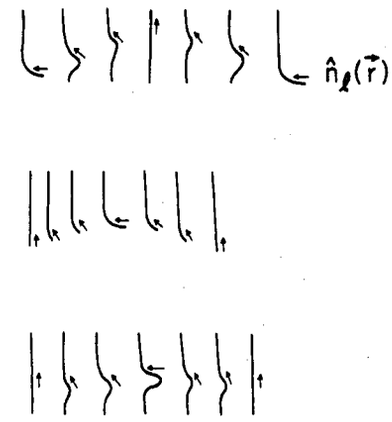

Figure 10. Illustrative examples for a collective distortion mode taking into account that the probability for defect formation increases as one proceeds down the chain toward the end methyl group. The small arrow denotes the orientation of $\hat{n}_l(\vec{r})$ corresponding to distorted chain segments.

We shall adopt the model of the continuous kink mode or chain reptation mode in interpreting our results. In order to discuss the spatial distribution for this model, we must consider the collective nature of the continuous kink mode: i.e., this process should be described as a "defect wave" propagating through the medium, rather than a single-chain process.

We have built a space-filling model of several DPPC molecules and created the smallest semicircle kink type deformation at some position along the chain by rotations about C–C bonds. We found that the mean chain length is not affected substantially by such deformations, and we also found that, assuming an all-trans configuration for the undeformed part of the chains, the fatty acid residues of neighboring molecules could approach each other as close as about 4–5 Å, whereas the two chains of one and the same molecule are nearly within close-packing distance. We again consider the $\theta = 0°$ orientation and define local directors $\hat{n}_l^c(\vec{r})$ for the solvent DPPC chains as the local tangents to the particular deformation at each location in the chain. Here θ' is the angle between $\hat{n}_l^c(\vec{r})$ and $\hat{n}_m$, while $\hat{n}_l^{NO}(\vec{r})$ denotes the tangent at the position of the NO group for DPPC bilayers doped with spin probe. In the case of 7,6-PC we would expect a close correspondence between $\hat{n}_l^{NO}(\vec{r})$ and the adjacent $\hat{n}_l^c(\vec{r})$. With $\hat{n}_l^c(\vec{r})$ obeying eq 4 so eq 1 is fulfilled, we describe the collective distortion mode, illustrated schematically in Figure 10, as follows. With $\theta' = 0°$ corresponding to an all-trans chain, we now assume that a deformation exists at some position along a particular chain, so that $\theta' \neq 0°$. This distortion is transmitted to an adjacent chain of the same molecule or of a neighboring one with an infinitesimal increase (or decrease) in amplitude. At some position $\vec{r}$ there is a maximum amplitude of distortion, i.e., $\theta' = 90°$. By continuing in the direction of this distortion wave to $\vec{r} + \vec{r}_1$, where $|\vec{r}_1| = P$ one complete wavelength is traversed. Since there is no reason for the defect wave to propagate in a particular direction within the bilayer plane all values equally of φ' are equally probable, e.g., the distortion waves in a particular bilayer could be correlated but the phases φ' for the different bilayers will most likely be random.

We recall now the cholesteric example of Luckhurst et al.[21] where an isotropic 2D distribution was obtained because all helix axes are perpendicular to $\vec{H}$; in our model the propagation directions y_l'' for the various defect wave

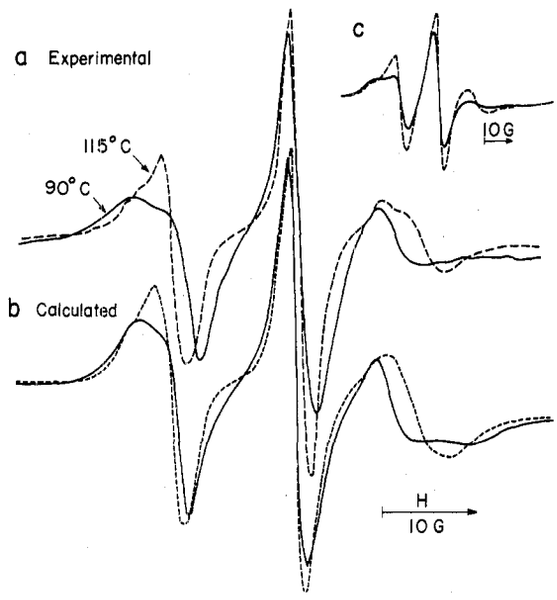

Figure 11. (a) ESR spectra of 10^{-3} M 7,6-PC dissolved in 2 wt% DPPC bilayers contained in a cylindrical tube sample holder at 90 (——) and 115 °C (---). (b) Calculated spectra with the parameters given in Tables I and II for 90 (——) and 115 °C (---). (T_2^{-1} was calculated with the values of $R_\perp$ corresponding to these temperatures from Table II and T_2^{*-1} from Table III.) The distribution function used to obtain these line shapes was $P(\theta',\varphi') = 1/4\pi$. (c) ESR spectrum of the 16-ketostearic acid label incorporated into purple membranes from halobacterium halobium at 25 (——) and 37 °C (---). (Reprinted with permission from ref 27. Copyright 1975 Academic Press.)

planes are, for $\theta = 0°$, all perpendicular to $\vec{H}$ due to the uniform alignment of the bilayers. Suppose this alignment of the y_l'' being perpendicular to $\vec{H}$ were destroyed. In the case of cholesterics, it was shown by Luckhurst[21] that addition of sufficient cholesterol chloride solute to the cholesteric rendered the ESR spectrum characteristic of an isotropic 2D spatial distribution into an isotropic 3D distribution. For the DPPC multilayers we would expect a change from a 2D powder pattern obtained for $\theta = 0°$ to a 3D powder pattern upon replacing the parallel glass plates by a cylindrical sample tube. This is based on the assumption that the effect of changing the geometry of the sample holder will be the creation of bilayer fragments distributed at random in the tube as compared to uniform bilayer alignment between parallel glass plates. This prediction is borne out by the experiment, as illustrated in Figure 11.

The spectra in Figure 11a are experimental spectra of tube samples of DPPC bilayers doped with 7,6-PC at 95 and 115 °C, and those in Figure 11b were calculated with $P(\theta',\varphi') = 1/4\pi$ and the parameters obtained from the simulations of the spectra from the plate samples for the same temperatures (see Table II). The fit between theory and experiment is seen to be good.

ESR line shapes bearing a striking similarity to our tube spectra have been reported by Chignell and Chignell[27] (see Figure 11c) who used the *N*-oxyl-4',4'-dimethyloxazolidine derivative of 5-ketostearic acid, 12-ketostearate and 16-ketostearate to probe the molecular organization of "purple membranes" isolated from halobacterium halobium. Their ESR spectra were interpreted in terms of a superposition of immobilized probe molecules bound to bacteriorhodopsin, which is the only protein present in the membrane, and mobile probes dissolved in a "free" fluid phase.

These systems are conformationally similar to our 7,6-PC tube samples and based on the similarity between the calculated spectra in Figure 11b and the experimental spectra of Chignell and Chignell (Figure 11c) we suggest an alternative interpretation in terms of a single species of ordered and mobile spin label molecules dissolved in the boundary phospholipid layer coating the bateriorhodopsin. The powderlike appearance of the ESR line shape would then be due to substantial microscopic order but macroscopic disorder and relatively fast motion rather than slow motion for a fraction of the spin probes. The implication of a highly mobile boundary lipid bilayer is consistent with a recent ESR spin label study of Davoust et al.[28] of maleimide labels bound covalently to rhodopsin in rhodopsin-egg lecithin vesicles. These authors pointed out the low microviscosity of the boundary lipids for high (500:1 mole to mole) lipid to protein ratio. It has been also reported by Davoust et al.[28] that upon lowering the temperature (or decreasing the lipid to protein ratio) powderlike features become visible in the spectrum and these were interpreted in terms of a second species of immobilized labels coexisting with the mobile species. However, "powderlike features", i.e., resonances at higher and lower fields may appear in the ESR spectrum as a consequence of increasing microscopic ordering of a mobile species (this trend is illustrated in Figure 11b) or as a result of motional effects for a side chain bound to a macromolecule,[18] e.g., a spin label bound covalently to a protein which is involved in faster internal motion about a mean symmetry axis of the binding site and slower overall reorientation of the entire complex. These possibilities should be critically explored as alternatives to the "two species" model.

We discussed above the expected behavior for 7,6-PC, which is identical with the host DPPC molecules except for the five-membered nitroxide ring attached to the eighth methylene carbon atom (counting from the carbonyl carbon). For this flexible probe it is reasonable to assume that the 7,6-PC chains also participate in the collective defect mode. Similar comments apply to the 12-doxylstearic acid probe which is a derivative of stearic acid (see Figure 1). On the other hand, the similarity of the ESR spectra of the two mainly rigid probes CSL and ADL to those of the flexible probes, implying that all the probe molecules are affected in a similar manner by the collective defect mode, is a direct manifestation of very strong lateral cooperativity of a hydrophobic nature. CSL possesses a branched chain residue attached to a rigid cholesterol-type core; however, ADL is built of a rigid core only. The ESR spectra of CSL and ADL are similar, except for a pronounced smearing of the main features in the ADL spectra relative to the CSL spectra. We interpret this difference by assuming that lateral cooperative forces operate mainly between aliphatic chains and therefore the coupling of the orientation of the local CSL director $\hat{n}_l^{NO}(\vec{r})$ to the surrounding local orientations of deformed DPPC chains $\hat{n}_l^{c}(\vec{r})$ is stronger than for ADL, whose "looser" coupling gives rise to an additional ("random") distribution of the local ADL directors $\hat{n}_l^{NO}(\vec{r})$ relative to the neighboring $\hat{n}_l^{c}(\vec{r})$. These results are relevant to the theory of interaction between the lipid molecules and between lipid molecules and various membrane components,[29a] in particular cholesterol derivatives, both diamagnetic and paramagnetic.[29b]

Finally, our model is consistent with the locally uniaxial environment of PD-Tempone since in the upper portion of the aliphatic chains, close to the carbonyl carbon, the probability of defect formation is small.[23] Also, we wish to note that the ESR spectra observed for CSL in the $L_\alpha(1)$ phase of uniform DPPC bilayers are similar to those observed for the same probe dissolved in an oriented smectic B_c phase of terephthalbis(butylaniline)[30a] (see Figure 4,a and c) and in the smectic phases of some 4-methoxybenzilidene-4'-amino-*n*-alkylcinnamates[30b] suggesting that

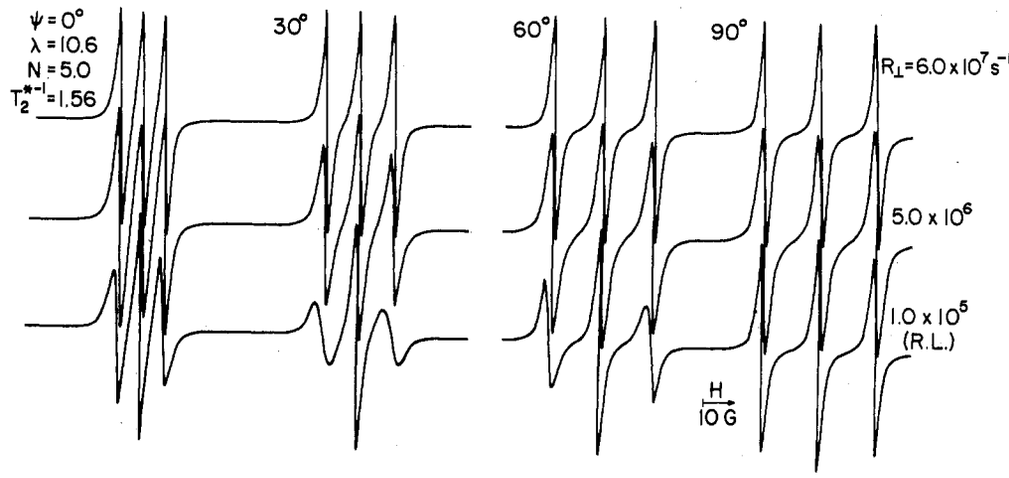

Figure 12. Calculated ESR spectra for a "fictitious" axially symmetric nitroxide with $a_{\parallel} = a_y'''$ and $a_{\perp} = {}^1/_2(a_x''' + a_z''')$ (a_x''', a_y''', and a_z''' denoting the principal values of the hyperfine tensor of CSL) and values of Ψ, λ, N, T_2^{*-1}, and $R_{\perp}$ as denoted in the figure. $R_{\perp} = 1.0 \times 10^5$ s^{-1} is the rigid limit (RL) value.

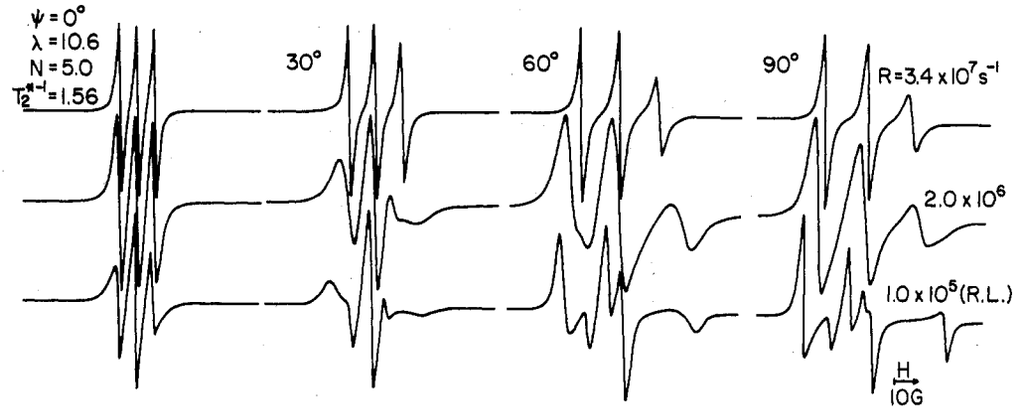

Figure 13. Calculated ESR spectra for CSL for y''' ordering with the magnetic parameters from Table I and Ψ, λ, N, T_2^{*-1}, and $R_{\perp}$ as denoted in the figure. $R_{\perp} = 1.0 \times 10^5$ yields the RL.

cooperative distortions are likely to be present in low temperature thermotropic smectic phases.

(2) *Homogeneous Broadening.* In this section we shall discuss the homogeneous line broadening which determines, at leaast in part, the line shapes of the individual components in the powder-type spectra. We have used a recently developed computer formulation of Moro and Freed,[4b] based on previous theories of Freed and coworkers[1,3,4] which enables one to calculate angular-dependent (i.e., $\theta \neq 0°$) ESR line shapes of a nitroxide radical in the presence of an axially symmetric ordering potential over the entire dynamic range from the fast to the slow tumbling limit. This formulation has been found to be very useful for our spectral analysis. In particular, for the case of very high ordering, as prevails in low water content DPPC bilayers, one predicts line shapes bearing some very distinctive features.

Since both 7,6-PC and 12-doxylstearic acid exhibit z''' ordering (i.e., $z''' = z$), the hyperfine tensor **A** is axially symmetric in the ordering frame. On the other hand, for y''' ordering (i.e., $y''' = y$) corresponding to CSL and ADL, **A** is nonaxial in the ordering frame. We find that for the high ordering observed (for CSL in the biaxial phase, $\lambda = 10.6$), the slow motional line shapes are affected substantially by the symmetry of **A** in the ordering frame and display very unique features, which we would like to illustrate in the following. To do this, we consider CSL with $\lambda = 10.6$, as well as a "CSL analogue" which is a fictitious axially symmetric nitroxide with $a_{\parallel} = a_y'''$ and $a_{\perp} = {}^1/_2(a_x''' + a_z''')$ with x''', y''', and z''' denoting the principal axes of the real CSL hyperfine tensor. The line shapes for the entire dynamic range of the "CSL analogue" and of CSL are illustrated in Figures 12 and 13. The main features characteristic of the very high ordering are the narrowness of the lines over the entire dynamic range for the "CSL analogue" for any orientation and the fact that the fast motional limit, wherein the spectrum becomes independent of motion, is attained at a rate $R_{\perp} = 6 \times 10^7$ s^{-1} which is much smaller than for isotropic solvents, while the lower limit occurs at $R_{\perp} = 1.0 \times 10^5$ s^{-1} which is an order of magnitude lower than for isotropic solvents. Also, the relatively small homogeneous broadening is probably the main reason for the sensitivity of the spectra to the shape of the distribution function.

Features similar to those described above are displayed by the 0° spectra computed for CSL in Figure 13. On the other hand, orientations other than $\Psi = 0°$ and in particular the $\Psi = 90°$ spectra become substantially spread out in field as the motion slows down, since $a_{x'} \neq a_{y'}$. The dynamic range for the 90° spectra extends from $R_{\perp} = 3.4 \times 10^9$ to 1×10^5 s^{-1} (for a reasonable intrinsic line width $T_2^{*-1} = 1.5$ G).

For 7,6-PC and 12-doxylstearic acid the z''' ordering was found to be lower than for CSL and typical theoretical spectra for these types of probes shown in Figure 14 illustrate the sensitivity of the intermediate orientations to slow motional effects.

To include the effects of homogeneous line broadening into our line-shape simulations we proceeded as follows. The degree of ordering can be estimated from the extreme

Figure 14. Calculated ESR spectra for 7,6-PC with the magnetic parameters from Table I for the $L_\alpha(1)$ phase. $\lambda = 3.8$, $\rho = 0.0$, $N = 4.0$, $z' \parallel z'''$, $T_2^{*-1} = 1.5$ G, and Ψ and $R_\perp$ as denoted in the figure.

TABLE III: Intrinsic Line Widths

	Ψ, deg	T_2^{*-1} [a]	T_2^{-1} $(m_I = +1)$	T_2^{-1} $(m_I = 0)$	T_2^{-1} $(m_I = -1)$
CSL in $L_\alpha(1)$ (107 °C)	0	1.5	1.5	1.5	1.5
	90	1.65	1.65	1.66	1.79
7,6-PC in $L_\alpha(1)$ (105 °C)	0	1.5	1.5	1.5	2.05
	90	1.4	1.4	1.42	1.69
12-doxylstearic acid in $L_\alpha(1)$ (107 °C)	0	0.8	1.2	1.5	1.0
	90	0.7	1.0	1.4	0.9
CSL in biaxial (40 °C)	0	1.8	1.77	1.8	1.84
	90	2.0	2.20	2.44	4.29
7,6-PC in biaxial (71 °C)	0	3.5	3.74	3.62	4.8
	90	3.4	5.37	3.4	7.87

[a] The trends in the angular dependence of T_2^{*-1} are similar to those observed in T_2^{-1}, in agreement with the results of Hemminga[30] on CSL in an equimolar mixture of DPPC and cholesterol and of Rao et al.[3a] on CSL in phase V. The accuracy in T_2^{*-1} is approximately 15%.

splitting in the experimental spectra, as though the Brownian motion were fast, (for very high ordering this is a good approximation for slower motions as well). From earlier simulations valid for the fast motional region, we were able to show that CSL obeys axially symmetric ordering, while 7,6-PC and 12-doxylstearic acid exhibit only small deviations from axial symmetry. Thus we assumed axially symmetric ordering in our detailed simulations. We then calculate, for values of λ close to the estimated values, the orientation-dependent line shapes for a particular rate $R_\perp$ s^{-1} letting $R_\perp$ span the entire dynamic range. The powderlike θ-dependent spectra are then simulated by superimposing a particular series of orientation-dependent line shapes corresponding to a particular value of $R_\perp$. The value of $R_\perp$ is then determined by a visual best fit procedure between calculated and experimental spectra. The other parameters entering the calculation, namely $N = R_\parallel/R_\perp$ (with $R_\parallel$ and $R_\perp$ denoting the principal components of an axially symmetric diffusion tensor), T_2^{*-1} denoting the intrinsic line width, and $\hat{N} = \hat{R}_\parallel/\hat{R}_\perp$ (with $\hat{R}_\parallel$ and $\hat{R}_\perp$ denoting the principal values of an axially symmetric viscosity tensor) were also varied to improve the fit. We shall discuss below the sensitivity of the ESR line shape to the various parameters.

The accurate approach for introducing the homogeneous line broadening into the calculation of the overall ESR lineshape is to calculate the line shapes of a large number of orientations Ψ and to superimpose these by using the appropriate distribution function. We have used an approximate approach based on the following arguments. First, in most cases only those orientations Ψ which are close to 0 and 90° contribute substantially to the observed powder patterns. Then, for all the highly ordered probes in the $L_\alpha(1)$ phase and for CSL in the biaxial phase (we shall discuss 7,6-PC in the biaxial phase separately) the line shapes corresponding to the individual orientations Ψ usually consist of a well-defined triplet enabling one to define an overall line width T_2^{-1} for each hyperfine component.

In all such cases the computer results[4b] yield a set of three dominant (complex) eigenvalues and eigenvectors which characterize the three-line nitroxide spectrum to a reasonably good approximation even for slower motions. The imaginary parts of the eigenvalues give the $T_2^{-1}(d)$, the dynamic line width contribution, while the real parts give the line positions. The overall width was taken to be $T_2^{-1} = T_2^{*-1} + T_2^{*-1}(d)$ where T_2^{*-1} the residual width determined mainly by unresolved proton superhyperfine interactions (but possibly also by some sample mosaicity, see below) and both T_2^{*-1} and $T_2^{-1}(d)$ are dependent on θ. The best fit values for T_2^{*-1} and T_2^{-1} are summarized in Table III. Despite the fact that T_2^{-1} was in some cases not much greater than T_2^{*-1} (e.g., CSL), still the final simulations, even for those cases, were rather sensitive to the choice of dynamical parameters, a matter we discuss below.

The T_2^{-1} values were found to increase upon going from $\Psi = 0°$ to $\Psi = 90°$ for CSL and ADL and to decrease for 7,6-PC and 12-doxylstearic acid. For convenience we used the analytical function $T_2^{-1} = a + b \cos^2 \psi$ for each hyperfine component with $a = T_2^{-1}(90°)$ and $a + b = T_2^{-1}(0°)$ to interpolate between 0 and 90°.

All line shapes, both in the $L_\alpha(1)$ phase and in the biaxial phase, were simulated with $P(\theta',\phi')$ given by eq 1. We refer below briefly to specific probes in the two phases. First we comment on fitting the magnetic tensors and then on fitting the dynamical parameters.

Magnetic Tensors. The principal values of the magnetic tensors for the various probes were estimated as follows. The a_N were measured in the isotropic phase occurring above $L_\alpha(1)$ and were compared with values found in similar systems utilizing the same (or similar) spin probes and for which the magnetic tensors are known. Based upon a comparison of the a_N values we used the scaling procedure as described by Lin and Freed[4a] and illustrated in section IIIA for PD-Tempone in the $L_\alpha(1)$ phase. Whenever further adjustment was necessary, we allowed for independent changes in the values of the individual com-

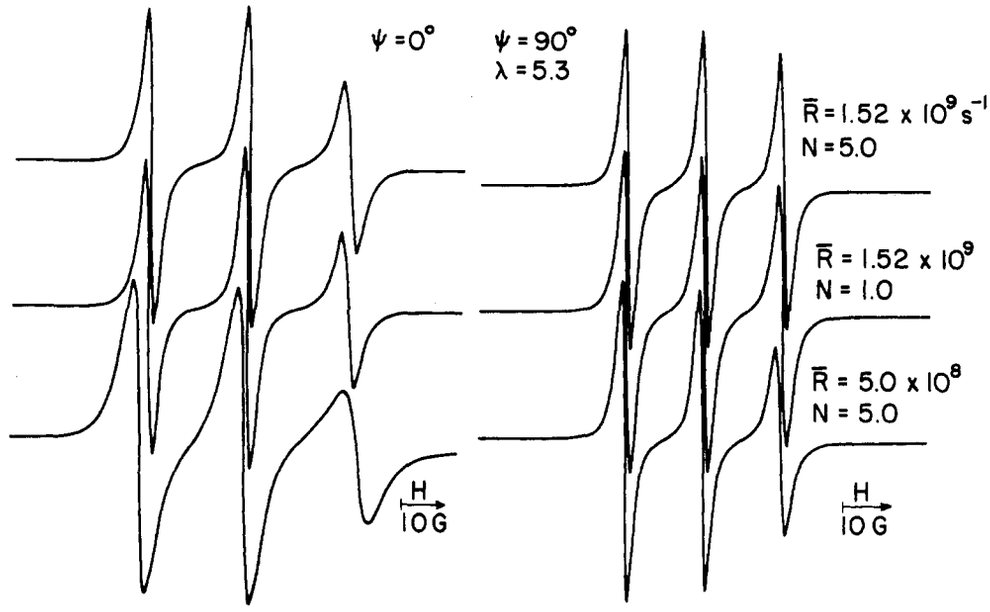

Figure 15. (a) Calculated spectra corresponding to CSL in $L_\alpha(1)$ for $\Psi = 0$ and 90° with the magnetic parameters from Table I, T_2^{*-1} for 107° from Table III, and $\bar{R} \equiv (R_\perp R_\parallel)^{1/2}$, N and λ as denoted in the figure. The T_2^{-1} values corresponding to the top trace were used to calculate the line shapes in Figure 4b.

ponents; we consider such cases as indicative of specific interactions, most likely steric interactions on the nitroxide moiety. It is largely because the orientation-dependent ($\theta \neq 0°$) spectra are so sensitive to the choice of magnetic parameters that we could carry out such a procedure. In fact we found that a complete line-shape analysis for our spectra was much more sensitive than one might initially expect from the analogous motionally narrowed formulas for splittings as a function of θ (cf. ref 4a).

For 7,6-PC and 12-doxylstearic acid in the $L_\alpha(1)$ phase we obtained good fit between theory and experiment (see Figures 5 and 6) by adopting the principal values of the hyperfine tensor corresponding to a nitroxide-labeled fatty acid immobilized by the lyophilized protein BSA given in Table I, Appendix IV, p 570 of ref 17 (see Table I). The principal values of the **g** tensor from this source were used without any further change to obtain reasonable fits for 7,6-PC in the biaxial phase (see Figure 8). On the other hand, the principal values of the hyperfine tensor had to be altered for this phase, as shown in Table I.

There seems to be a correlation between the details of interaction of the 7,6-PC probe molecules with the surrounding DPPC molecules and their state of motion. The collective nature of the distortion mode is indicative of cooperative lateral interactions, but presumably does not involve the nitroxide moiety in the $L_\alpha(1)$ phase. The considerable slowing down of the overall molecular reorientation in the biaxial phase is probably accompanied by intermolecular interactions, involving also the nitroxide moiety, as indicated by the substantial changes in the principal values of the hyperfine tensor when the liquid crystalline–gel phase transition is crossed.

For CSL we first tried to use the values of the magnetic tensors for this probe in brain lipid[3a] but found that further variation in these values (not necessarily by the scaling procedure) was required both in the $L_\alpha(1)$ and in the biaxial phase. The final values used in the calculations are given in Table I.

As already mentioned, failure to use the scaling procedure is believed to indicate specific interactions of the nitroxide moiety (e.g., steric strains). Problems of phospholipid–solute interaction have been addressed from a theoretical point of view. Also, the possibility of various membrane components binding to the phospholipid molecules has been implied by various experimental findings.[29]

Dynamic Parameters. For CSL in $L_\alpha(1)$ we have calculated orientation-dependent line shapes for various rates $R_\perp$, with λ ranging from 5.00 to 5.50, T_2^{*-1} from 1.0 to 2.0 G, and $1.0 \leq N \leq 7.0$. We found that in this range the line shapes are relatively insensitive to N and we chose $N = 5.0$ as predicted by the molecular geometry of CSL. The best visual fit between the overall calculated line shape and their experimental counterparts were obtained for values corresponding to the various parameters summarized in Tables II and III and the fit for 107 °C is illustrated in Figure 4. We illustrate in Figure 15 the (unexpected) sensitivity of the spectra to $\bar{R} \equiv (R_\parallel R_\perp)^{1/2}$ and the relative insensitivity to the value of N.

For 7,6-PC in the $L_\alpha(1)$ phase, the best fit with the experimental spectra for various temperatures was obtained with the parameters summarized in Tables I–III and is illustrated in Figure 6 for 105 °C.

The overall line shapes for 12-doxylstearic acid were obtained following the procedure outlined above with the best fit parameters given in Tables I–III. The fit for 107 °C is illustrated in Figure 5.

Although the spectral resolution for CSL decreases upon going from $L_\alpha(1)$ to the biaxial phase, this effect is compensated to some extent by the high sensitivity of the $\Psi = 90°$ spectra to $\bar{R}$ (see Figure 13). We find that CSL is not immobilized in the biaxial phase and is very highly ordered (see Table II). Again, the parameters in Tables II and III were used to calculate the overall line shape as illustrated in Figure 7 for 40 °C.

For 7,6-PC in the biaxial phase we found that the line widths of the individual hyperfine components are of the order of 3.5–5.5 G. We have calculated line shapes corresponding to T_2^{-1} of this order of magnitude using the parameters in Tables I and II and T_2^{*-1} from Table III. As a general trend, we notice that the line widths decrease for all the hyperfine components by going from $\Psi = 0°$ to $\Psi = 90°$. The spectra for intermediate values of Ψ display more complex features but these contribute to the overall line shape to only a very small extent. We have measured the distance between the extrema in the derivatives for the

individual hyperfine components both for $\Psi = 0°$ and for $\Psi = 90°$ and used these values as empirical line widths T_2^{-1}. Obviously, this is an approximate approach appropriate for purely Lorentzian lines. However, we found that the fit obtained this way for rates close to the rigid limit values was good, as shown in Figure 8 for 71 °C. This result indicates that in the biaxial phase 7,6-PC is probably immobilized on the ESR time scale (i.e., the sensitivity to the exact value of $\bar{R}$ in this range is very low). We also found that the ESR spectrum of 7,6-PC in the biaxial phase is very nearly invariant to further reduction in the temperature.

Mosaicity. We have not explicitly included in our calculations effects of inhomogeneous line broadening due to mosaicity in the sample. In the $L_\alpha(1)$ phase we obtained good fits between calculated and experimental spectra for all probes, and we therefore conclude that the mosaicity effects are small [i.e., contained within the $T_2^*(\theta)^{-1}$]. The problem is likely to be amplified in the biaxial phase for two reasons. First, Stomatoff et al.[11a] found with X-ray crystallography a mosaic spread as great as 15° (full-width at half-maximum) in the biaxial phase. Second, the approximate approach of defining an empirical line width from the calculated spectra for the individual line width is even more questionable in the biaxial phase than in the $L_\alpha(1)$ phase due to the asymmetry of the slow motional spectra. However, the good fit between the calculated and the experimental spectra in Figures 7 and 8 is suggestive of a relatively small contribution of the mosaicity.

We have interpreted the ESR line shapes for 7,6-PC in the biaxial phase by assuming that the spectra of the individual sites for each Ψ are rigid-limit spectra obtained by freezing in a smectic ordering described by $\lambda = 3.8$ as noted above. This is equivalent to a distribution of instantaneous ordering axes z' relative to $\hat{n}_l(\vec{r})$. Alternatively, one might consider this disorder as arising from a Gaussian-type distribution about z_l'' due to mosaicity. While it is not possible to differentiate between these two cases from the ESR spectra alone, it is not reasonable to assume that we can obtain consistently "good" biaxial crystals for the CSL-doped bilayers but highly mosaic crystals for the 7,6-PC-doped DPPC bilayers. Furthermore, we found that in order to obtain a mosaicity equivalent to the distribution implied by the function $e^{-3.8 \sin^2 \Psi}$, one has to assume a mosaic spread of a characteristic half-width of about 31°. This is definitely inconsistent with the results obtained with CSL (and other probes) in the biaxial phase. We therefore conclude that our interpretation of having a rigid smectic ordering is reasonable.

The various parameters determined in our line-shape simulations are summarized in Tables II and III together with the appropriate accuracy limits. The ordering potential parameter λ could be determined with relatively high accuracy, since it determines the field positions of the various peaks and these were found to be very sensitive to small variations in λ. On the other hand, the uncertainty in T_2^{*-1}, $\bar{R}$, and N is greater, mainly due to the number of parameters involved in the calculation and their similar effect on the line shape. We also present in Table II estimates for the activation energies.

Other Comments. We would like to comment on a particular feature in the experimental spectra of both CSL and 12-doxylstearic acid illustrated in Figures 4 and 6, namely, a considerable contribution to the $\theta = 60°$ spectrum from intermediate orientations Ψ (cf. Figure 13) which could not be reproduced with the calculations described above.

We have explored the possibility of a magnetic-field-induced redistribution of z_l'' axes relative to z_m'' upon tilting the field away from the $\theta = 0°$ orientation, using a distribution function of the type

$$P(\theta,\theta',\varphi') = \frac{(1 - k^2 \cos^2 \Psi)^{-1/2}}{\int_0^{2\pi} (1 - k^2 \cos^2 \Psi)^{-1/2} \, d\Psi} (\sin \theta')^{-1}$$

which is a slight generalization of the form proposed by de Gennes[31] to describe field-induced distortions and used by Luckhurst et al.[21] to analyze $\theta = 0°$ ESR spectra from a cholesteric phase. Note for $k = 0$ this is again eq 1. However, we could not reproduce the feature mentioned above with any value of $0 \leq k \leq 1$. We believe that the substantial contribution to the ESR line shape from particular intermediate orientations might be a line width effect, related to the angular dependence of T_2^{*-1}. Hemminga[32] found that the residual or inhomogeneous line width of CSL dissolved in a mixture containing equimolar quantities of DPPC and cholesterol exhibits a minimum for an intermediate orientation Ψ, which cannot be explained with a $(3 \cos^2 \Psi - 1)$ type angular dependence of the superhyperfine splittings. A nonmonotonic variation in the value of T_2^{*-1} as a function of orientation has been also observed for CSL in the solid state,[32] and a similar effect in the $L_\alpha(1)$ phase will indeed be manifested in our powderlike spectra in terms of higher intensity from intermediate orientations.

IV. Further Remarks. Relation to Other Work.

In view of our ESR results with the hydrophobic probes, one might be tempted to consider a morphology other than lamellar bilayers, e.g., layers consisting of DPPC molecules arranged in a rodlike manner with a cylindrical symmetry axis that is random for the different layers. Such models are, however, contrary to our results with the head-group probes showing smectic-A type alignment. They are also inconsistent for the same reason with the ^{31}P NMR results of Griffin et al.[13b] on these oriented multilayers. Also, such structures are expected to be very unstable energetically for very low water-content due to the large radius of curvature of the rods.

Furthermore, X-ray[11] and neutron diffraction[12] measurements appear to be clearly indicative of the lamellar structure. In particular, we note that the neutron diffraction results show a rather well-localized distribution of ^2H atoms close to the polar interface (i.e., near the carbonyl carbon) in the $L_\alpha(1)$ phase showing that this position is well ordered. However, near the end-methyl groups there is a significant increase in the distribution representing considerable disorder.

Our ESR results are consistent with this disorder being due to the cooperative chain distortions. We find in part 2[33] of this series that in the biaxial phase the ESR spectra of PD-Tempone do reflect a similar type of cooperative disorder as the hydrophobic probes in the $L_\alpha(1)$ phase. This is consistent with the observation by neutron diffraction[12b] that there is substantial disorder over the entire chain length in the biaxial phase. This indicates that, in the biaxial phase, the upper chain region is also experiencing local (but coperative) disorder again consistent with the neutron diffraction results.[12c]

There is an alternative explanation to the absence of any effects of the cooperative distortion on the PD-Tempone spectra in the $L_\alpha(1)$ phase, but one that we think is less likely. This is the possibility that the PD-Tempone (or Tempamine) translates by fast enough diffusion to average out the effects of the distortions. This explanation would still be consistent with the overall lamellar structure.

Actually, one would expect diffusion in the low water content phases (especially for 2% H_2O) to be quite slow, although no relevant experiments appear to have been performed.[34] While the PD-Tempone spectra for the biaxial phase do show evidence for cooperative distortions, the VO^{2+} ions, which are likely bound to the PO_4^- of the headgroup, do not show any such effect[33] in accord with the aspect of our proposed model, wherein the headgroups are not appreciably affected by the distortions.

Further evidence on the head-group behavior in the biaxial phase given in part 2 does clearly indicate that headgroup probes and hydrophobic probes do not behave in a similar manner, since only the former exhibit magnetic-field-induced orientational effects.

In the $L_\alpha(1)$ phase our model does require that the DPPC chains do reorient fairly readily relative to the local direction $\hat{n}_1(\vec{r})$ in a manner such that the effects of $\hat{n}_1(\vec{r})$ are not transmitted to the headgroup, and this appears feasible from examination of molecular models. Also the various ESR probes show dynamical features that closely reflect the dynamics of their surroundings. Of particular interest in this regard is the fact that the observed activation energies for reorientation for all the probes in the $L_\alpha(1)$ phase are, within experimental uncertainty, the same (cf. Table II) as well as the same as that determined more accurately for headgroup motion from ^{31}P NMR (for 14% water content in the biaxial phase).[35] It is possible that in the freezing out of such chain motions there is at least some transmission of the effects of the distribution in the $\hat{n}_1(\vec{r})$ for the chains to the headgroups.

We also take note of the fact that our results for PD-Tempone in the $L_\alpha(1)$ phase are very similar in many respects to the observations of Lin and Freed[4a] on this probe in the smectic B_A phase of the thermotropic liquid crystal 40,6. Thus, in the two cases one finds the ordering is invariant with temperature and furthermore the magnitude and asymmetry of the ordering are very nearly the same. Also, the motions in both cases exhibit anomalies we attribute to SRLS. Differences are in the slower motional rates in DPPC host and the larger a_N in the latter as already discussed.

On the other hand, we have noted that CSL probe in smectic B_C phases exhibit spectral features similar to this probe in the $L_\alpha(1)$ phase of DPPC and this is supportive of the existence of similar cooperative chain distortions in these thermotropic phases.

V. Conclusions

The following conclusions have been reached:

(1) ESR spectra of spin probes in oriented multilayers of DPPC are sufficiently well resolved to determine accurate distribution functions for the local ordering.

(2) The ESR spectra from hydrophobic probes clearly show a distinctive cooperative type of distribution that could be distinguished from random types of distributions.

(3) The weakly aligned head-group probes show smectic A type of alignment in the $L_\alpha(1)$ phase, which is consistent with a uniaxial local environment of the bilayer.

(4) These results are interpreted in terms of cooperative chain distortions in these media.

(5) Further studies with spin-labeled DPPC with the nitroxide moiety at different positions along the chain *and* the headgroup would be very desirable.

Acknowledgment. We acknowledge support for this research by NSF Grant No. DMR77-17510 and NIH Grant No. GM 25862-02. E. M. is thankful for a Chaim Weizmann Fellowship (1977–9). We thank Dr. Winston Chan for his advice on the preparation of well-aligned DPPC multilayers and Dr. Giorgio Moro for his extensive help with the complex spectral simulations.

References and Notes

(1) (a) C. F. Polnaszek, G. V. Bruno, and J. H. Freed, *J. Chem. Phys.*, **58**, 3185 (1973); (b) C. F. Polnaszek and J. H. Freed, *J. Phys. Chem.*, **79**, 2273 (1975); (c) J. H. Freed in "Spin-Labeling: Theory and Application", L. J. Berliner, Ed., Academic Press, New York, 1976, Chapter 3.
(2) G. R. Luckhurst and A. Sanson, *Mol. Phys.*, **24**, 1297 (1972); G. R. Luckhurst in "Liquid Crystalline Systems", Vol. 2, G. W. Gray and A. A. Winsor, Ed., Ellis Harwood, New York, 1974, Chapter 7.
(3) (a) K. V. S. Rao, C. F. Polnaszek, and J. H. Freed, *J. Phys. Chem.*, **81**, 449 (1977); (b) J. S. Hwang, R. P. Mason, L. P. Hwang, and J. H. Freed, *ibid.*, **79**, 489 (1975).
(4) (a) W. J. Lin and J. H. Freed, *J. Phys. Chem.*, **83**, 379 (1979); (b) G. Moro and J. H. Freed, *J. Phys. Chem.*, **84**, 2837 (1980); (c) E. Meirovitch and J. H. Freed, to be submitted for publication.
(5) R. J. Birgeneau and J. D. Litster, *J. Phys. Lett.*, **39**, L-399 (1978).
(6) (a) J. Charvolin and B. Mely, *Mol. Cryst. Liq. Cryst. Lett.*, **41**, 209 (1978); (b) J. Charvolin and A. Tardieu, *Solid State Phys., Suppl.* **14**, 209 (1978); (c) J. Seelig, *Q. Rev. Biophys.*, **10**, 353 (1977).
(7) (a) R. Kimmick and A. Peters, *J. Magn. Reson.*, **19**, 144 (1975); (b) A. de Vries, *Mol. Cryst. Liq. Cryst.*, **49**, 19 (1978).
(8) (a) J. Seeliger, R. Osredkar, V. Zagar, and R. Blinc, *Phys. Rev. Lett.*, **38**, 411 (1977); J. Seeliger, V. Zagar, and R. Blinc, *Phys. Rev. A*, **17**, 1149 (1978); (b) A. J. Dianoux and F. Volino, *J. Phys.*, **40**, 181 (1979), and references cited therein; (c) A. M. Levelut, *J. Phys.*, **37**, 13-C51 (1976).
(9) (a) L. Powers and P. S. Pershan, *Biophys. J.*, **20**, 137 (1977); (b) L. Powers and N. A. Clark, *Proc. Natl. Acad. Sci. U.S.A.*, **72**, 840 (1975); (c) L. Powers, Thesis, Harvard University, 1977.
(10) (a) S. A. Asher and P. S. Pershan, *Biophys. J.*, **27**, 393 (1979); (b) *J. Phys.*, **40**, 161 (1979).
(11) (a) J. B. Stomatoff, W. F. Graddick, L. Powers, and D. C. Moncton, *Biophys. J.*, **25**, 253 (1979); (b) J. Stomatoff, T. Bilash, Y. Ching, and P. Eisenberger, *Ibid.*, **28**, 413 (1979); (c) A. Tardieu, V. Luzzati, and F. C. Reman, *J. Mol. Biol.*, **75**, 711 (1973).
(12) (a) G. Buldt, H. V. Gally, A. Seelig, and J. Seelig, *Nature (London)*, **271**, 182 (1978); (b) G. Zaccai, G. Buldt, A. Seelig, and J. Seelig, *J. Mol. Biol.*, **134**, 693 (1979); (c) G. Buldt, H. U. Gally, J. Seelig, and G. Zaccai, *Ibid.*, **134**, 673 (1979).
(13) (a) R. G. Griffin, *J. Am. Chem. Soc.*, **98**, 851 (1976); (b) R. G. Griffin, L. Powers, and P. S. Pershan, *Biochemistry*, **17**, 2718 (1978).
(14) (a) W. L. Hubbell and H. M. McConnell, *J. Am. Chem. Soc.*, **93**, 314 (1971); (b) E. G. Rozantsev, "Free Nitroxyl Radicals", Plenum Press, New York, 1970.
(15) (a) A. D. Keith and D. Chapman, *Biochemistry*, **16**, 634 (1977); (b) S. Schreier, C. F. Polnaszek, and I. C. P. Smith, *Biochim. Biophys. Acta*, **515**, 375 (1978); (c) C. F. Polnaszek, Sh. Schreier, K. W. Butler, and I. C. P. Smith, *J. Am. Chem. Soc.*, **100**, 8223 (1978).
(16) S. J. Kohler and M. P. Klein, *Biochemistry*, **16**, 519 (1977).
(17) L. J. Berliner, Ed., "Spin Labeling-Theory and Applications", Academic Press, New York, 1976.
(18) R. P. Mason, C. F. Polnaszek, and J. H. Freed, *J. Phys. Chem.*, **78**, 1324 (1974).
(19) J. Seelig and H. Limacher, *Mol. Cryst. Liq. Cryst.*, **25**, 105 (1974).
(20) A. Abragam and B. Bleaney, "Electron Paramagnetic Resonance of Transition Ions", Clarendon Press, Oxford, 1970, p 200.
(21) G. L. Luckhurst and H. J. Smith, *Mol. Cryst. Liq. Cryst.*, **20**, 319 (1973).
(22) E. Meirovitch, Z. Luz, and S. Alexander, *Mol. Phys.*, **37**, 1489 (1979).
(23) S. Hsi, J. Zimmerman, and Z. Luz, *J. Chem. Phys.*, **69**, 4126 (1978).
(24) G. T. Evans, *J. Chem. Phys.*, **69**, 3363 (1978); R. Kimmick, *Polymer*, **18**, 233 (1977).
(25) D. F. Bocian and S. I. Chan, *Annu. Rev. Phys. Chem.*, **29**, 307 (1978).
(26) P. G. de Gennes, *J. Chem. Phys.*, **55**, 572 (1971); P. G. de Gennes, *Macromolecules*, **9**, 587 (1976); S. Daoudi, *J. Phys.*, **38**, 731 (1976); J. P. Cohen-Addad, *Ibid.*, **39**, C2-175 (1978); K. Bergmann, *J. Polym. Sci.*, **16**, 1611 (1978).
(27) C. F. Chignell and D. A. Chignell, *Biochim. Biophys. Res. Commun.*, **62**, 136 (1975).
(28) J. Davoust, B. M. Schoot, and Ph. F. Devaux, *Proc. Natl. Acad. Sci. U.S.A.*, **76**, 2755 (1979).
(29) (a) Y. Lange, J. S. D'Alessandro, and D. M. Small, *Biochim. Biophys. Acta*, **556**, 388 (1979); (b) E. Tipping, B. Ketterer, and L. Christodoulides, *Biochem. J.*, **180**, 319 (1979); H. C. Jarrell, R. Deslauriers, W. H. McGregor, and I. C. P. Smith, *Biochemistry*, **19**, 385 (1980).
(30) (a) E. Meirovitch and Z. Luz, *Mol. Phys.*, **30**, 1589 (1975); (b) D. Sy and M. Ptak, *J. Phys.*, **35**, 517 (1974); *Mol. Cryst. Liq. Cryst.*, **39**, 53 (1977).
(31) P. G. de Gennes, *Solid State Commun.*, **6**, 163 (1968).
(32) M. Hemminga, *Chem. Phys.*, **6**, 87 (1974).
(33) E. Meirovitch and J. H. Freed, *J. Phys. Chem.*, following paper in this issue.
(34) We can attempt an order of magnitude estimate of the requirements on the diffusion coefficient D, that it be too small to average any effects of distortion modes. First we estimate R_{eff} for such a process. For small angular jumps, $\delta\theta$ we have $R \approx (\delta\theta)^2/6\delta\tau$ (cf. ref 1c), while

$D \approx (\delta r)^2/6\delta\tau$ using isotropic motion for simplicity. Then from eq 2 we obtain (with $\delta y \rightarrow \delta r$ for simplicity), $R_{\text{eff}} \approx 4\pi^2 D/P^2$. Now, for a nitroxide, the slow tumbling region is for $\tau_R \equiv (6R)^{-1} \gtrsim 10^{-8}$ s. But since we have $\langle D_\omega^2 \rangle \sim 0.1$ (cf. Table II), then in the present case we have $\tau_R \gtrsim 10^{-8}$ s^{-1}. Thus, motional averaging of the distortion effect would require $P^2/24\pi^2 D < 10^{-8}$ s. E.g., for $D \approx 10^{-8}$ (10^{-6}) cm^2/s, we would require a $P < 15$ (150) Å. A value of $P < 15$ Å seems very unlikely, since it is then of the order of the average dimension of a DPPC molecule, while $P < 150$ Å is not as unlikely but would require a rather fast D.

(35) R. F. Campbell, E. Meirovitch, and J. H. Freed, J. Phys. Chem., 83, 525 (1979).

ESR Studies of Low Water Content 1,2-Dipalmitoyl-*sn*-glycero-3-phosphocholine in Oriented Multilayers. 2. Evidence for Magnetic-Field-Induced Reorientation of the Polar Headgroups

Eva Meirovitch and Jack H. Freed*

Baker Laboratory of Chemistry, Cornell University, Ithaca, New York 14853 *(Received: May 6, 1980)*

In this continuation of ESR studies on a variety of spin probes incorporated into low-water-content 1,2-dipalmitoyl-*sn*-glycero-3-phosphocholine (DPPC) bilayers, results with the headgroup-region probes, PD-Tempone and VO^{2+}, are reported for the biaxial phase. The fluidity of the weakly ordered PD-Tempone probe is quite high for higher water content (14 wt %) but decreases for lower water content (9 wt %) (i.e., $R_\perp$, the diffusion coefficient, decreases from 10^9 to 10^8 s^{-1} and shows properties probably related to slowly relaxing local structure in the latter case). The VO^{2+} ions are, however, immobilized on the ESR time scale and weakly oriented. Both probes show distributions in local director, which, however, become better aligned as $\vec{H}$, the magnetic field, is tilted into the bilayer plane. Also both probes then have a preferential alignment perpendicular to the projection of $\vec{H}$ in this plane. These results are taken as definite evidence for cooperative headgroup alignment by the magnetic field. While positive (vs. negative) diamagnetic susceptibility is expected they could not be distinguished by these experiments. Anomalous results from a stearamide probe in the $L_\alpha(1)$ phase, viz. an unusually large observed splitting of 19.05 G with plate samples but typical splitting of 16.1 G with tube samples, is taken as evidence for significant differences in microscopic ordering properties of the DPPC samples resulting from different anchoring constraints imposed by the shapes of the holders. The nature of the biaxiality observed in the biaxial phase by other techniques is considered in the light of these ESR results.

I. Introduction

The addition of small amounts of water to dry phospholipids results in the formation of bilayer structures with a hydrophobic interior and two polar interfaces. In a preceding ESR spin-probe study (referred to in the following as 1)[1] we examined evidence for cooperative chain distortions taking place in the hydrophobic region of the bilayer; the subject of the present study is an examination of evidence for cooperative headgroup reorientation at the bilayer interface enhanced by external magnetic fields and by surface forces.

We studied 2–14 wt % water content DPPC both in the biaxial and in the $L_\alpha(1)$ phases, using the alignment technique of Powers and Pershan[2] to prepare uniform planar multilayers between parallel glass plates. In these aligned phases the main chain axes $\hat{d}_c$ of DPPC are perpendicular to the main headgroup axes $\hat{d}_h$ of the phospholipid molecules, and at low water content $\hat{d}_c$ is approximately parallel to $\hat{n}_m$, the normal to the plates and to the bilayers, implying that the $\hat{d}_h$ axes lie within the bilary plane, as illustrated in Figures 1 and 2.

Our ESR results on these phases show some distinctive and unusual characteristics for which we suggest interpretations relevant to an understanding of the physical properties of these phases. Thus we relate the phenomenon of magnetic-field-induced molecular reorientation, previously observed with model[3a] and biological[3b] membranes, to the molecular conformation of DPPC and to long-range cooperative alignment in the bilayer plane and between adjacent bilayers. We show that our results on the well-aligned DPPC samples are consistent with the hypothesis that, upon tilting the external field $\vec{H}$ away from $\hat{n}_m$, the DPPC headgroups reorient in the bilayer plane so as to optimize the angle between $\hat{d}_h$ and $\vec{H}$.

Surface-aligning forces are likely to contribute substantially to the long-range alignment of the headgroups. By replacing the parallel glass surfaces by a cylindrical sample holder, the boundary conditions are drastically altered. In support of this we find with a stearamide spin probe in the $L_\alpha(1)$ phase that by changing the sample geometry, not only the macroscopic alignment, but also the microscopic characteristics, as reflected in the ESR spectra of this probe, are substantially altered. Our findings with this probe (which is built of a stearic acid chain residue and a piperidine ring containing the nitroxide) are consistent with a hypothesis that in the plate samples the piperidine ring is intercalated between adjacent bilayers and with high ordering and probably experiences "very anisotropic" diffusion, whereas in tubes the familiar behavior[4] of low ordering and slightly anisotropic diffusion is encountered. Such a description would be consistent with a considerable decrease in the extent of lateral as well as interbilayer cooperativity in the latter case, while in the former the plates tend to layering which imposes rather severe conformational and dynamic restrictions on the stearamide molecule.

We do suggest that a cooperative in-plane "anchoring" of headgroups may be achieved in the plate samples during the growth process of the biaxial phase from the higher $L_\alpha(1)$ phase, inducing a nonzero biaxial birefringence. This

0022-3654/80/2084-3295$01.00/0